THESIS FOR THE DEGREE OF LICENTIATE OF ENGINEERING

GaN HEMT Based Highly Integrated Active Antenna Element for Millimeter-Wave Array Transmitters

WAN-CHUN LIAO

CHALMERS
UNIVERSITY OF TECHNOLOGY

Department of Electrical Engineering
Chalmers University of Technology
Gothenburg, Sweden, 2020

GaN HEMT Based Highly Integrated Active Antenna Element for Millimeter-Wave Array Transmitters
WAN-CHUN LIAO

Department of Electrical Engineering
Chalmers University of Technology
SE-412 96 Gothenburg
Sweden
Telephone: +46 (0)31-772 1000
www.chalmers.se

Typeset using LaTeX.

Printed by Chalmers Reproservice
Gothenburg, Sweden 2020

To family and friends

GaN HEMT Based Highly Integrated Active Antenna Element
for Millimeter-Wave Array Transmitters

Wan-Chun Liao
Department of Electrical Engineering
Chalmers University of Technology

Abstract

Next-generation wireless technology (5G) promises a digital transformation enabled by enhanced mobile broadband and low latency communication, which can reshape the ways of working and living in the future. The demand in high data capacity and throughput requires a technological revolution. 5G aims to achieve data rates in the order of gigabit per second in the lower band of the millimeter-wave spectrum ($<40\,\mathrm{GHz}$). At these frequencies, multi-antenna systems with a vast number of highly integrated active antennas are necessary to deliver energy-efficient and cost-effective technological solutions to enable future 5G applications.

Nowadays, there is a lack of accurate antenna-circuit analysis tools. An interdisciplinary co-optimization methodology is proposed in this thesis. A K-band GaN HEMT power amplifier-integrated active antenna was optimized with the methodology to directly match the transistor output to its optimal load impedance while taking account of the nonlinear behavior of active devices and the over-the-air coupling effects in the vicinity of the transition between the amplifier and the antenna. Direct match obviates the need for a potentially lossy and bandwidth-limited output impedance matching network. The presented active antenna element is compact ($0.6\,\lambda \times 0.5\,\lambda$), high-gain (active antenna gain of $15\,\mathrm{dBi}$), and energy-efficient (peak power-added efficiency of $49.5\,\%$). The proposed methodology can solve some major challenges of next-generation wireless communication technology.

To further implement the proposed interdisciplinary methodology, one needs to understand the mutual coupling effects between the ports at the same element and different elements in a multiport integrated active array antenna. Today, the studies on the mutual coupling effects are mostly for passive antenna arrays or active antenna arrays of assuming a single-port reference impedance. A scattering parameters re-normalization procedure is presented in this thesis to account for the interaction effects in power amplifier-integrated array antennas. This technique provides an insightful interpretation of the mutual coupling coefficients of power waves in integrated array antennas.

Keywords: Active integrated antenna, co-design, energy-efficient, GaN HEMT, mutual coupling, millimeter-wave, power amplifier.

List of Publications

This thesis is based on the following publications:

[A] **Wan-Chun Liao**, Rob Maaskant, Thomas Emanuelsson, Martin Johansson, Anders Höök, Johan Wettergren, Michael Dieudonne, Marianna Ivashina, "A Ka-Band Active Integrated Antenna for 5G Applications: Initial Design Flow". *Published in IEEE 2nd URSI AT-RASC*, May 2018.

[B] **Wan-Chun Liao**, Rob Maaskant, Thomas Emanuelsson, Vessen Vassilev, Oleg Iupikov, Marianna Ivashina, "A Directly Matched PA-Integrated K-band Antenna for Efficient mm-Wave High-Power Generation". *Published in IEEE Antennas Wirel. Propag. Lett*, Nov. 2019.

[C] **Wan-Chun Liao**, Rob Maaskant, Thomas Emanuelsson, Artem Vilenskiy, and Marianna Ivashina, , "Antenna Mutual Coupling Effects in Highly Integrated Transmitter Arrays". *Accepted in Proc. 14th Eur. Conf. on Antennas and Propag. (EuCAP)*, Copenhagen, Denmark, Apr. 2020..

Other publications by the author, not included in this thesis, are:

[D] R. Maaskant, O. A. Iupikov, C. A. H. M. van Puijenbroek, **W.-C. Liao**, M. Matters-Kammerer, M. V. Ivashina, "Deep Integration Antenna Array: Design Philosophy and Principles". *Proc. 13th European Conference on Antennas and Propagation (EuCAP)*, Krakow, Poland, Apr. 2019.

[E] I. Aziz, **W.-C. Liao**, H. Aliakbari (In press), "Compact and Low Cost Linear Antenna Array for Millimeter Wave Automotive Radar Applications". *Proc. 14th European Conference on Antennas and Propagation (EuCAP)*, Copenhagen, Denmark, Apr. 2020.

[F] J. Fan, K. Zhu, J. Yang, H. Yuan, P. Jiang, Y. Yan, **W.-C. Liao**, H. Cao, J. Ma, B. Li, "Design of Novel Flat Bend Crossed Dipole for Wideband Phased Array Feed Applications". *Proc. 2019 International Symposium on Antennas and Propagation (ISAP)* Xian, China, Oct. 2019.

[G] J. Fan, J. Yang, Y. Yan, **W.-C. Liao**, D. Zhan (Submitted), "Investigation of Ultrawideband Bowtie Antennas for Phased Array Feed Application". *International Journal of RF and Microwave Computer-Aided Engineering* .

Acknowledgments

I want to thank Vinnova for funding the ChaseOn project *Integrated Array Antennas (iAA)*, and thank Ericsson, Saab, Ruag Space, Gapwaves, and Keysight for supporting this project. I would also like to acknowledge KTH Royal Institute of Technology for collaborating in this project.

I wish to express my sincere appreciation to my main supervisor, Professor Marianna V. Ivashina, for her constant guidance and great support. I also want to thank my co-supervisor, Associate Professor Rob Maaskant, for being a great discussion partner when I need it. I wish to show my gratitude for my co-supervisor, Adjunct Professor, Thomas Emanuelsson, for the stimulating whiteboard sessions. I want to pay my special acknowledgments to Associate Professor Vessen Vassilev for his valuable support on integrated module design and measurement.

I wish to thank Bluetest, especially Robert Rehammar, for letting us use the facility for measurement. I also want to pay my special regards to Oleg Iupikov for the generous assistance on measurements and post-processing.

I wish to show my gratitude to all the support to all the colleagues at the Department of Electrical Engineering, especially to Abbas, Artem, Jinlin, Madeleine, Morteza, Navid, Sadegh, Samar, and Tomas for all the delightful times. Huge thanks go to Madeleine and Sadegh for proofreading this thesis.

To my friends and family, I want to thank you for being supportive and encouraging, especially to Kuan-Lun, for your unconditional support. Special acknowledgments to Roxie for being lovable and soothing my mind. Last, I want to express my deepest gratitude to Abby for always being there; I could not have gone this far without your support.

—Wan-Chun C. Liao

Acronyms

5G:	Fifth Generation
ADS:	Advanced Design System
AIA:	Active Integrated Antenna
AIAiP:	Active-Integrated-Antenna-in-Package
AiP:	Antenna-in-Package
AMC:	Artificial Magnetic Conductor
AoC:	Antenna-on-Chip
AP:	Access Point
BiCMOS:	Bipolar Complementary Metal Oxide Semiconductor
CMOS:	Complementary Metal-Oxide-Semiconductor
DRC:	Design Rule Checking
DUT:	Device Under Test
EIRP:	Equivalent Isotropic Radiated Power
EM:	Electromagnetics
eMBB:	enhanced Mobile Broadband
FET:	Field-Effect Transistor
FWA:	Fixed Wireless Access
GaAs:	Gallium Arsenide
GaN:	Gallium Nitride
HBT:	Heterojunction Bipolar Transistor
HEMT:	High Electron Mobility Transistor

IAB:	Integrated Access and Backhaul
IC:	Integrated Circuit
IMD:	Intermodulation Distortion
IMN:	Impedance Matching Network
IMT:	International Mobile Telecommunications
MC:	Mutual Coupling
MMIC:	Monolithic Microwave Integrated Circuit
mMTC:	massive Machine Type Communications
MU-MIMO:	Multi-User, Multiple-Input, Multiple-Output
mmWave:	Millimeter-Wave
OTA:	Over-The-Air
PA:	Power Amplifier
PAE:	Power-Added Efficiency
PAIAA:	Power Amplifier-Integrated Active Antenna
PCB:	Printed Circuit Board
SiGe:	Silicon-Germanium
SoC:	System-on-Chip
TOI:	Third-Order Intercept point
URLLC:	Ultra-Reliable and Low Latency Communications

Contents

Part I

Introductory Chapters

CHAPTER 1

Introduction

1.1 Motivation

The evolution of wireless communication has been substantially driving the socio-technical growth for the last few decades, which has contributed to socio-economic development all over the world. Next-generation wireless technology, commonly known as 5G (fifth generation), is defined by three major usage scenarios of International Mobile Telecommunications (IMT)-2020 [1]: enhanced Mobile Broadband (eMBB), Ultra-Reliable and Low Latency Communications (URLLC), and massive Machine Type Communications (mMTC), as shown in Figure 1.1. With the dawn of the 5G era, a digital transformation, enabled by enhanced mobile broadband and low latency communications, is taking place in almost every industry, which can reshape our ways of working and living.

The continuously increasing demand in data capacity and throughput for the next-generation wireless communication requires a technological revolution to accomplish the broadband capabilities of mobile networks and the advanced wireless connectivity for the major usage scenarios. This revolution can drive new technological solutions into the microwave and millimeter-wave (mmWave) frequency domain [3]. At these frequencies, the available bandwidths can be in the order of gigahertz that can enable

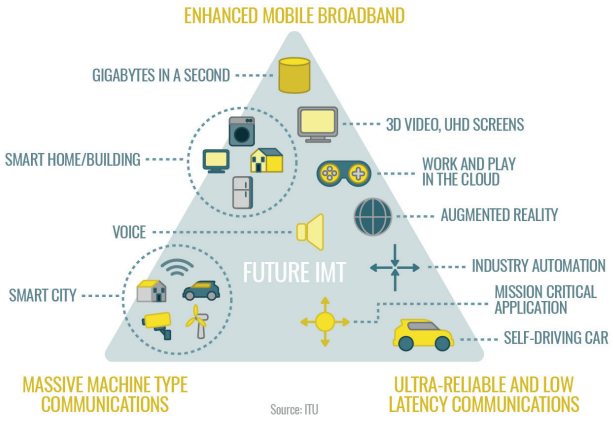

Figure 1.1: Usage scenarios of IMT for 2020 and beyond [2].

both high system capacity and high data rate, which is improbable to be realized in the conventional cellular sub-6 GHz bands due to the limitations of existing technology.

The wireless connectivity of the communication system is constrained by its link budget, taking account of all the power gains and losses in a communication system, and the fundamental factor—the operating frequency. The *Friis Transmission Equation* relates the power received to the power transmitted between two antennas separated by a distance $R > 2D^2/\lambda$, where D is the largest dimension of either antenna, and λ is the wavelength. The ratio of the received to the transmitted power (P_r and P_t) can be written as

$$\frac{P_r}{P_t} = \eta_t \eta_r \frac{\lambda^2 D_t(\theta_t, \phi_t) D_r(\theta_r, \phi_r)}{(4\pi R)^2} = \frac{\lambda^2 G_t(\theta_t, \phi_t) G_r(\theta_r, \phi_r)}{(4\pi R)^2} \tag{1.1}$$

where η_t, η_r are the radiation efficiency, D_t, D_r are the directivity, and G_t, G_r are the gain of the transmitting and receiving antennas in the direction θ_t, ϕ_t and θ_r, ϕ_r[1], respectively [5]. The term $(4\pi R/\lambda)^2$ is called the *free-space path loss (FSPL)*, and it takes into account the losses due to the propagation between the transmitting and receiving antennas. Suppose all the transmitter and the receiver hardware remains identical, increasing operating frequency leads to increased FSPL considering the FSPL between the transmitter and receiver is proportional to the frequency squared

[1] In a spherical coordinate system, (r, θ, ϕ) gives the radial distance, polar angle, and azimuthal angle.

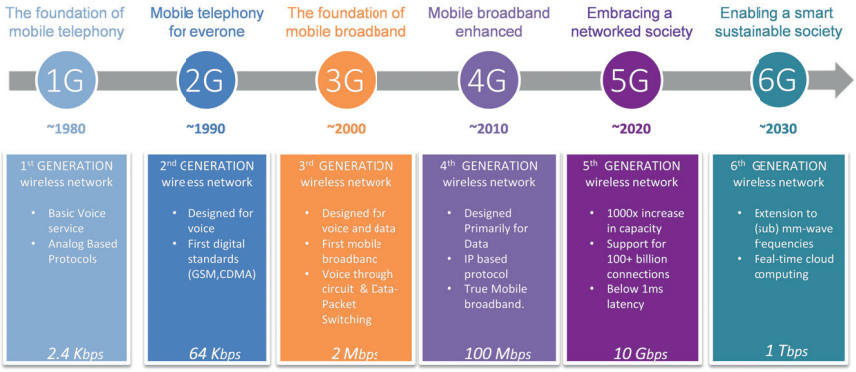

Figure 1.2: Roadmap towards 5G and beyond 5G wireless communication systems [4].

($\lambda = c/f$, c is the speed of light in free space, and f is the operating frequency). The two most intuitive solutions to improve the link budget at mmWave frequencies are shortening communication distance and increasing antenna gain and output power. The former is often undesirable or even impractical (e.g., satellite communications), and therefore increasing the antenna gain and transmitted power at the transmitter is the clear choice of solution to compensate for the additional loss in link budget at higher frequencies. Consequently, array antennas integrated with front-end electronics that provide increased system gain and digital beamforming over wide scan angles are considered as critical components in future mmWave wireless communication systems.

The roadmap towards 5G and beyond 5G is shown in Figure 1.2. 5G aims to achieve data rates up to $10\,\mathrm{Gbit/s}$ through the use of the mmWave spectrum in the lower band ($<40\,\mathrm{GHz}$). At these frequencies, multi-antenna systems with a vast number of highly integrated active antennas are necessary to overcome the substantial path loss between base-station and mobile user equipment. Beyond 5G even exploit frequencies above $100\,\mathrm{GHz}$. The system efficiency of the current transmitter solutions is inferior, commonly below $30\,\%$ around $30\,\mathrm{GHz}$.

Energy-efficient and cost-effective technological solutions are needed to enable the IMT future applications, especially, innovative solutions to issues of highly integrated components/sub-systems and its manufacturability. Compact and cost-effective physical realization (so-called *building practice*) is needed for mmWave integrated array antenna systems with many transceivers and antenna elements [6]. Integrated front-

end electronics must be confined within the cross-section of the aperture of the antenna element or the sub-array of elements to enable modularity and cost-effective designs. Considering the substantially reduced footprint of antennas in mmWave frequency (scaled with wavelength), innovative interdisciplinary design methodologies are demanded to address the complex interrelation between the linearity, power efficiency, heat dissipation, and output power of active sub-systems at the transmitting end. The array mutual coupling (MC) between the power amplifier (PA) of integrated antenna elements also needs to be evaluated as the active load impedance that varies dynamically can affect the system performance [7]. Therefore it is imperative to exploit joint design and optimization of the integrated front-end electronics and radiating elements to minimize the MC and enhance performance over solutions of optimizing the sub-components separately.

Furthermore, the physical antenna ports of integrated systems at mmWave frequencies are either not available or not accessible; thus, the conventional characterization approach of testing the sub-systems (e.g., the radiating elements and the PAs) separately is not applicable. Hence the over-the-air (OTA) characterization of the integrated array antenna system becomes crucial. The challenges and solutions of characterizing an active integrated antenna (AIA) in an anechoic chamber (line-of-sight environment) and a reverberation chamber (rich isotropic multipath environment) were discussed in [8].

1.2 Design challenges in millimeter-wave wireless communication

Much attention has been drawn to overcome the technical barriers to cost-effectively leverage the vastly available bandwidth at mmWave frequencies and satisfy the future demands. The challenges of simulation, design, integration, physical realization, packaging, and testing of complete systems are different and more complicated than today's wireless communication systems, as well as the cost needs to be kept at the same level as today's wireless systems. Considering the wavelength, the level of integration complexity exceeds the sub-6 GHz range.The conventional circuit and antenna design techniques are not necessarily accurate and lead to suboptimal design and performance in the mmWave spectrum. For instance, a microstrip feed line is commonly used in the circuit and antenna design at lower frequencies due to its low-cost, low-profile, and well-established characteristics. However, specific problems of microstrip lines start to surface when designing in this frequency range. Among these

problems are the conductor and dielectric losses that increase with frequency. Also, microstrip lines with large areas or discontinuities can lead to a spurious influence on the radiation patterns. One must investigate those potential issues properly to alleviate the adverse effects. Additionally, the choice of the substrate can have a considerable impact on antenna efficiency [9]. Circuit and antenna designers must consider the design trade-offs, including the cost, system performance, miniaturization, and physical realization.

1.3 5G application domains

Apart from the IMT applications, three specific application domains are presented in this research project: *space-based communications*, *defense-oriented applications*, and *terrestrial cellular wireless communications*. A brief domain overview and the use cases are shown for each domain, and a set of aligned integrated array antenna system constraints are listed in Table 1.1. The system constraints are provided by the industrial project partners within the ChaseOn centre, including Ericsson, RUAG space, SaaB, and Gapwaves [10].

1.3.1 Space-borne communications

One emerging field for space-borne communication using integrated array antennas is high capacity telecommunication systems at Ka-band, using a 30-GHz uplink and a 20-GHz downlink. Of particular interest is the downlink, a transmitting system on Geostationary Earth Orbit (GEO) spacecraft, as shown in Figure 1.3.

1.3.2 Defense applications

A brief technological perspective is given for applications in public safety and national security. In these domains, there is a rapidly growing interest in small array antenna systems intended for either fixed installations (mounted on walls or masts) or for small, unmanned mobile platforms (Unmanned aerial vehicles [UAVs], road vehicles, and boats), see Figure 1.4. These array antenna systems should be able to execute sensing and communication functions. In general, the interplay between the antenna element and the densely packed transmitter and receiver electronics for array antenna systems in the 12 GHz to 40 GHz and even beyond these frequency bands is expected to be in focus for antenna research for the next ten years.

Figure 1.3: A GEO satellite with four array-fed reflectors (Eutelsat/Thales Alenia Space *Broadband for Africa* High Throughput Satellite) [11].

Figure 1.4: UAV with conformal integrated array antenna in the fuselage [12], [13].

1.3.3 Terrestrial cellular communications

Array antennas are essential components in mmWave communications systems, with features that combine to improve the overall system performance. The antenna gain can be increased by using directive beamforming, hence providing improved system coverage. Similarly, interference can be reduced by the spatial filtering effect of directed beams. For multi-layer communication, beamforming can exploit channel diversity to minimize cross-talk between the different layers in spatial multiplexing systems with, for example, multi-user, multiple-input, multiple-output (MU-MIMO). Array antennas having integrated front-end electronics and digital or hybrid beamforming allow frequency-dependent beamforming. Besides, they also avoid some of the efficiency (loss) issues in traditional systems, in which the transmitted RF signal from one or a few power amplifiers needs to be routed to each element.

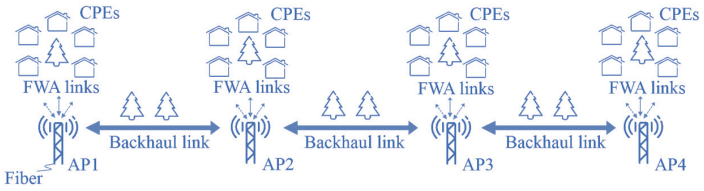

Figure 1.5: Illustration of a multi-hop FWA system with access-integrated backhaul. The APs serve both the CPEs located at the residential houses and provide backhaul to neighboring APs. AP1 has a dedicated fiber connection [14].

Use case—Integrated access and backhaul (IAB) in 5G One example enabled by the wide bandwidths at mmWave frequencies is in a fixed wireless access (FWA) network [14]. The backhaul is fully integrated with the access, and the frequency band, radio interface, and radio resources, including hardware, are shared by the access and backhaul connections. Such technology is called the *access-integrated backhaul* system in an FWA. In the evaluated FWA deployment, each residential house connects its consumer premises equipment to an access point (AP). By using multi-hop backhaul with universal frequency reuse (all nodes use the same frequency) between the APs in a time-division duplex system, only a fraction of the APs needs to be connected to fiber backhaul, as shown in Figure 1.5. The main advantages of such a system are rapid deployment and significantly reduced cost since the need for locations with access to fiber is reduced.

Aligned System constraints

A commonly aligned list of constraints has been tailored based on the three 5G application domains, as shown in Table 1.1.

1.4 Millimeter-wave active integrated antenna technologies

Many solutions have been investigated in front-end circuitry-antenna integration design for mmWave frequency applications, such as *antenna-on-chip (AoC)*, *antenna-in-package (AiP)*, and *hybrid concept*. The definition and overview of these technologies are introduced in this section.

Table 1.1: Aligned system constraints derived from three 5G application domains for integrated array antennas at mmWave frequencies.

Performance Metrics & Design Parameters	Constraints
Array aperture area	10–100 λ^2
Array configuration	planar array*; $\sim \lambda/2$
Radiating element	dual-polarized
Frequency band	20–40 GHz†
Bandwidth	5–10 %
Instantaneous bandwidth	1–5 %
Beamforming	digital
Scan angle	$\pm 60^\circ \times \pm 60^\circ$ (EL×AZ)‡
Peak output power per element	15–25 dBm
Isolation between PAs at output	-15 dB
Noise figure	5–7 dB
Total power efficiency	>25 %

* Planar array in rectangular grid.
† Not continuous.
‡ EL is the elevation angle; AZ is the azimuth angle.

1.4.1 Antenna On-Chip (AoC)

It is expected that the integration and miniaturization at mmWave would head to an entire system-on-chip (SoC) realization. SoC is appealing on account of low cost, reliability, reproducibility, and miniaturization. These characteristics promise affordable commercial wireless solutions. However, AoC and SoC developments are still in their infancy stage due to the design challenges. Complementary metal-oxide-semiconductor (CMOS) process is relatively cost-effective, and the mainstream technology for digital circuits; however, Figure 1.6 shows that silicon substrates are not optimal for antenna operation due to its low resistivity (ρ = 1–20 Ω-cm) and high permittivity ($\epsilon_r = 11.9$). Low resistivity leads to ohmic loss that turns into heat dissipation. High permittivity and thick substrate trigger substrate modes that can severely affect antenna radiation performance and cause additional problems in an array system due to the surface wave coupling between adjacent elements. It is essential to understand the major contributor to the inferior AoC efficiency to resolve this issue

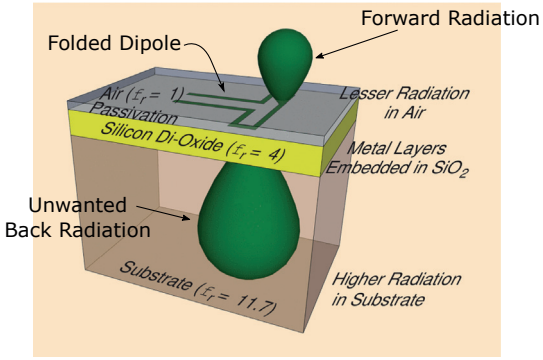

Figure 1.6: Electromagnetic (EM) radiation from AoCs in silicon-based technology [15].

effectively. Several techniques and related studies to enhance the AoC performance are:

- Substrate Thinning [16]–[18]
- Proton Implantation (increase substrate resistivity below AoC) [19]–[21]
- Micromachining (remove the substrate in proximity to AoC) [21], [22]
- Superstrate Focusing (additional part on the substrate to improve the performance) [23], [24]
- Electromagnetic (EM) Shielding (employs artificial magnetic conductor (AMC) to enhance AoC performance) [25]–[29].

Also, an evaluation of the fractional bandwidth of using AMC for AoC applications is performed in [30]. In the upper region of the mmWave frequency spectrum, the fractional bandwidth, while applying AMC in the metal stack of a CMOS process, looks promising, as shown in Figure 1.7.

There are other challenges in AoC design, e.g., the layout is dictated by the foundry specific rules, and there are no provisions for on-chip-antenna. Therefore, it is challenging to resolve design rule checking (DRC) errors; AoC characteristics can be influenced by packaging significantly, and it is challenging to take account of the effects.

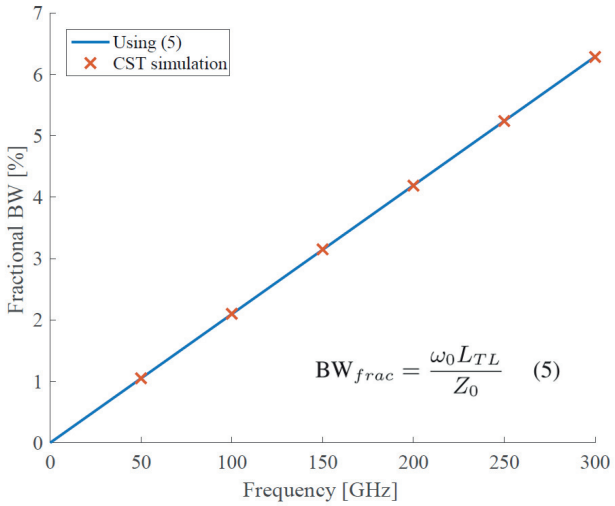

Figure 1.7: Evaluated fractional bandwidth versus frequency for applying AMC in the metal stack of CMOS process, where L_{TL} is the equivalent inductance of the transmission line, ω_0 is the resonance frequency, and Z_0 is the characteristic impedance of the medium above the AMC [30].

1.4.2 Antenna-in-Package (AiP)

AiP is another solution for integrated wireless communication array antenna systems. Currently, there is much interest in AiP technology for 5G New Radio (NR) [31]. Different from AoC, AiP can provide higher antenna performance with higher gain and efficiency, and low loss substrate. The AiP solution has a much shorter distance to the front-end circuit than a conventional discrete antenna. Shorter-interconnection suggests reduced transmission loss that can potentially enhance the efficiency of the transmitter and the noise figure of the receiver. Additionally, the AiP solution reduces system and assembly costs.

Nonetheless, AiP should be designed together with the front-end chip in the initial system architecture phase for optimum results. Moreover, one would prefer a well-confined EM environment for the AiP radiation. Thus the antenna performance is less sensitive to the carried package, printed circuit board (PCB) substrate, and metallic structures [32]. However, it is improbable to have good reliable designs without taking account of the interactive effects between the front-end chip and the AiP. The overall

system performance can become much worse than expected if these effects are neglected. When AiPs are jointly designed with the front-end circuits and implemented with a multidisciplinary circuit-antenna co-design methodology (*cf.* Section 2.3), one can take the interactive effects between the AiP and the front-end integrated circuit (IC) into consideration and mitigate the these issues.

1.4.3 Hybrid integrated mmWave antenna

An antenna integrated with the front-end IC but is neither implemented in the packaging technology nor in the IC back-end is referred to as *hybrid integrated antenna concept*, or short as *hybrid concept* [33]. Hybrid integration solution may not be as compact as the AoC nor the AiP solutions, but it has the extra design flexibility that the other two technologies cannot provide. The additional degree of freedom in design and optimization can become leverage in active antenna integration if used judiciously.

1.5 Goal and objectives

In view of the aforementioned motivation, this research project aims to ***develop new integration solutions for mmWave antenna arrays for various types of 5G applications***. Several objectives are established to achieve such aim:

1. Develop a multidisciplinary co-design flow and methodology capable of taking account of the critical effects of front-end electronics (e.g., amplifiers) in the integrated-antenna design process.

2. Investigate new integration concepts:

   i) use suitable off-the-shelf transistors,

   ii) design PAs in-house for integration,

   iii) aim at testbed demonstration.

Throughout this project, we aim to improve energy efficiency while having reduced form factor and production cost.

1.6 Thesis outline

Chapter 2 proposes the multidisciplinary co-design methodology and the integration concept of a highly integrated PA-integrated active antenna (PAIAA) element. An overview of the MC effects of antenna arrays is presented in **Chapter 3**, including a scattering parameter re-normalization procedure that is used to characterize the MC effects in integrated active antenna arrays. The summary of the included papers is shown in **Chapter 4**, and the papers are included in **Part II**. The conclusion and future work are presented in **Chapter 5**.

1.7 Terminology

Radiation Intensity U In a given direction, the power radiated from an antenna per unit solid angle **[IEEE Std 145-2013]**. U_o is the radiation intensity of an isotropic source.

Directivity $D_{\mathbf{ant}}$ Directivity of an antenna in a given direction is defined as the ratio of the radiation intensity in a given direction from the antenna to the radiation intensity averaged over all directions **[IEEE Std 145-2013]**. The average radiation intensity is equal to the total power radiated by the antenna (P_{rad}) divided by 4π. If the direction is not specified, the direction of maximum radiation intensity (maximum directivity) is implied.

$$D_{\text{ant}} = \frac{U(\theta,\phi)}{U_o} = \frac{4\pi U(\theta,\phi)}{P_{\text{rad}}}$$

Antenna Radiation Efficiency $\eta_{\mathbf{rad}}$ The ratio of the total power radiated by an antenna to the net power accepted by the antenna from the connected transmitter **[IEEE Std 145-2013]**.

Antenna Gain $G_{\mathbf{ant}}$ The ratio of the radiation intensity in a given direction to the radiation intensity that would be produced if the power accepted by the antenna (P_{in}) were isotropically radiated **[IEEE Std 145-2013]**.

$$G_{\text{ant}} = 4\pi\frac{U(\theta,\phi)}{P_{\text{in}}} = \eta_{\text{rad}}4\pi\frac{U(\theta,\phi)}{P_{\text{rad}}} = \eta_{\text{rad}}D_{\text{ant}}(\theta,\phi)$$

Equivalent Isotropically Radiated Power (EIRP) In a given direction, the gain of a transmitting antenna multiplied by the net power accepted by the antenna from the connected transmitter **[IEEE Std 145-2013]**.

$$\text{EIRP} = G_{\text{ant}}(\text{dBi}) + P_{\text{in}}(\text{dBW})$$

Active Antenna Gain G_{AIA} If a single RF input port were available then there was no fundamental reason that gain could not be defined in the standard way, and measured by comparing the signal power transmitted from the unknown antenna, with a given signal level applied to its input port, to the power transmitted by a gain-standard antenna, with the same signal input. This definition might result in a gain value substantially larger than the directivity because of the amplifier gain [34].

$$G_{\text{AIA}} = G_{\text{PA}} G_{\text{ant}}$$

Available Power Gain G_{a}

$$G_{\text{a}} = \frac{\text{the maximimum available average power at the load}}{\text{the maximum available average power at the source}} = \frac{P_{\text{out,max}}}{P_{\text{in,max}}}$$

Efficiency (of an AIA)

$$\eta_{\text{AIA}} = \frac{\text{the average power delivered to the load}}{\text{the average power drawn from the DC supply voltage}} = \frac{P_{\text{out}}}{P_{\text{DC}}} \times 100\%$$

Power Gain G_{P}

$$G_{\text{P}} = \frac{\text{the average power delivered to the load}}{\text{the average power delivered to the source}} = \frac{P_{\text{out}}}{P_{\text{in}}}$$

Power-Added Efficiency (PAE)

$$\begin{aligned}\text{PAE} &= \frac{\text{the average power delivered to the load} - \text{the average input power}}{\text{the average power drawn from the DC supply voltage}} \\ &= \frac{P_{\text{out}}}{P_{\text{DC}}} \times 100\%\end{aligned}$$

Transducer Power Gain $G_{\mathbf{PA}}$

$$G_{\text{PA}} = \frac{\text{the average power delivered to the load}}{\text{the average power available at the source}} = \frac{P_{\text{out}}}{P_{\text{acc}}}$$

Unconditional Stability The network is unconditionally stable if $|\Gamma_{\text{in}}| < 1$ and $|\Gamma_{\text{out}}| < 1$ for all passive source and load impedances (i.e., $|\Gamma_{\text{S}}| < 1$ and $|\Gamma_{\text{L}}| < 1$), where $\Gamma_{\text{in}}, \Gamma_{\text{out}}, \Gamma_{\text{S}}$, and Γ_{L} are the reflection coefficient seen looking toward the input, output, source, and load [35].

Conditional Stability The network is conditionally stable if $|\Gamma_{\text{in}}| < 1$ and $|\Gamma_{\text{out}}| < 1$ only for a certain range of passive source and load impedances. This case is also referred to as potentially unstable [35].

CHAPTER 2

Active Integrated Antenna (AIA) Element

An AIA overview, PA-antenna co-design, and co-optimization methodology are presented in this chapter, including an example of a PAIAA element characterized by the OTA procedure.

2.1 Overview of AIA design approaches

There are various definitions of the AIA in the literature [36], [38] that describe different levels of integration for the antenna system, as shown in Table 2.1. In the conventional type of antenna system, no integration is involved. The boundary between the sub-systems of the active circuit and the antenna is distinct. Thus, they are generally designed and analyzed by two teams of specialists (i.e., circuit and antenna designers individually), as shown in Figure 2.1. The individual teams need to transform the interface impedance to equal value (generally $50\,\Omega$) to interconnect the sub-systems smoothly, which is commonly realized by impedance matching networks (IMNs). These sub-systems are well-isolated because of the IMNs; however, the footprint of conventional designs is also bulky, and the power losses increase due to these networks. Therefore, such a conventional 50-Ω design is not suitable for large-scale arrays and mmWave frequency applications.

IMNs are obviated in the *high integration* approach to avoid the drawbacks mentioned above. Thus an active antenna of *high integration* can potentially have a smaller form factor and higher power efficiency than the conventional active antennas, especially at high frequency and wideband applications. Consequently, one needs to define an arbitrary interface impedance between the sub-systems because of the absence of the IMNs. The optimal system performance can be attained by customizing the interface impedance, which is generally not $50\,\Omega$. Hence, it is necessary to exploit a multidisciplinary co-design methodology that can be used to determine the optimal interface impedance and to design the active component and the radiating element

Table 2.1: AIAs categorized by different level of circuit-antenna integration.

Conventional 50Ω design	**High Integration**	**Deep Integration** [36], [37]
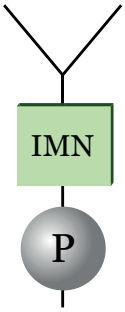	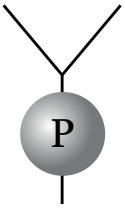	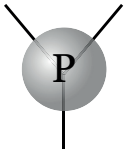
+ Well-isolated sub-systems/components + Well-established design approach – Bulky design and high power losses – Not suitable for large-scale arrays, and mmWaves	+ Customized interface impedance (no output IMN) + Lower profile and reduced power losses – Require multidisciplinary co-design	+ Active devices become part of radiating element + Higher degree of freedom in optimization – Complex integration design – Practical implementation – High risk of self-oscillation

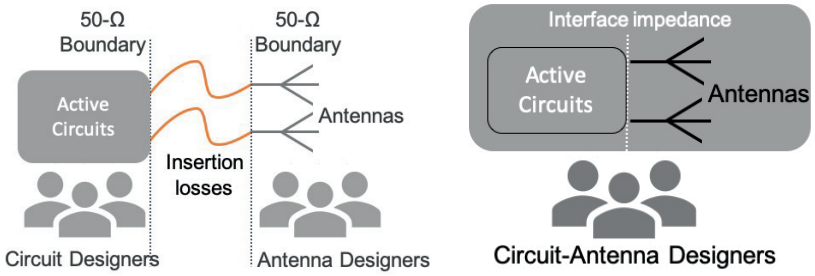

(a) (b)

Figure 2.1: (a) A traditional 50-Ω interface/boundary between circuit and antenna designers and (b) circuit-antenna integration with arbitrary interface impedance.

jointly. This methodology shall take into account all the critical interaction effects, such as *intra-element* and *inter-element* MCs (addressed in Section 3.1), and hence realize optimal system performance.

The *deep integration* concept incorporates the active component into the radiating element (inseparable) and consequently can provide the design with the smallest form factor. The designers can have a high degree of freedom in AIA optimization by adopting the *deep integration* concept. However, this type of integrated circuit-antenna module is complex and challenging to analyze since it requires joint EM-circuit analysis. That is, antenna designers need to equip inter-disciplinary skills and knowledge, such as monolithic microwave integrated circuits (MMICs) design and process, to be equal to a deeply integrated AIA. Practical implementation challenges are critical due to the lack of suitable manufacturing processes and a high risk of self-oscillation due to potential isolation issues.

Limitations of the conventional IMN in terms of insertion loss and bandwidth in the K-band frequencies were investigated in [39]. There are different contributions of insertion loss at the boundary of sub-systems, such as the losses in the conductor and dielectric materials, and radiation loss. Radiation loss results from the stray radiation of microstrip lines. The stray radiation can affect the antenna radiation pattern, result in undesired coupling and crosstalk, and deteriorate the thermal management problem. Figure 2.2 shows the insertion loss of the IMN with different bandwidths with respect to the theoretical case (the optimum power-added efficiency, $\mathrm{PAE}_{\mathrm{opt}} = 0\,\mathrm{dB}$).

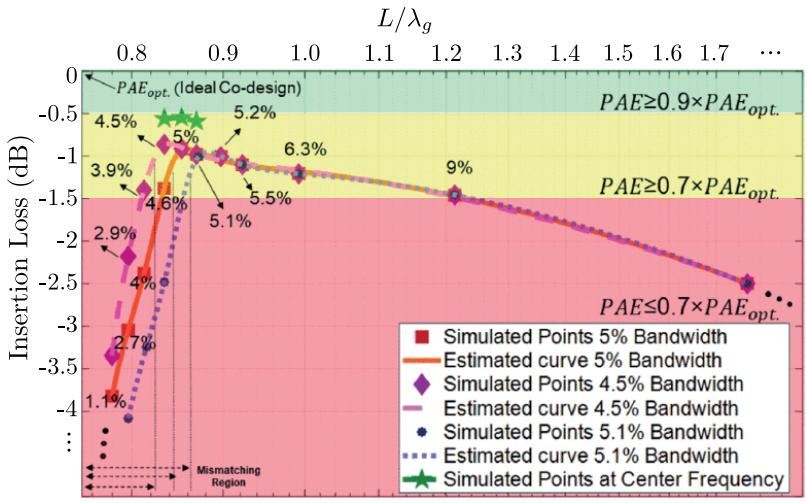

Figure 2.2: Insertion loss diagram versus the electric size where L is the length of output matching network [39].

Most designs, where the length of the matching network varies from 0.8 to $1.7\,\lambda_g$[1], have at least $30\,\%$ PAE loss compared to the optimum case. By using direct integration, it is probable to improve the PAE by $10\,\%$ over a $5\,\%$ frequency bandwidth, as shown in Figure 2.2, which reduces the insertion loss and thus enhances the system efficiency.

In conclusion, although providing good isolation between the sub-systems or discrete components, the conventional antenna is bulky and lossy and, therefore, not well-suited for mmWave large-scale active arrays. On the other hand, deeply integrated active antennas can likely provide the smallest form factor and least transition loss. Despite that, this level of integration also suggests a high risk of system self-oscillation due to that it is more challenging to analyze the inseparable AIA accurately. The *high integration* concept represents a good compromise in terms of the small form factor, high system efficiency, and manufacturability. Hence, we have selected the *high integration* concept in the present work.

[1] λ_g is the guide wavelength of the substrate.

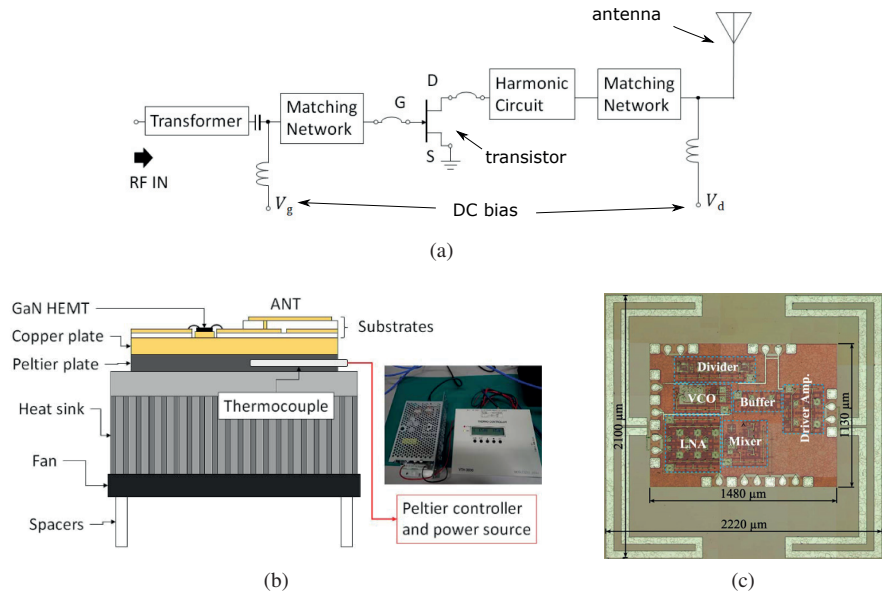

Figure 2.3: (a) GaN-active-antenna-circuit configuration. D, G, and, S indicate the transistor terminals [43]. (b) Active-antenna configuration on a Peltier cooling unit ($1.9\,\lambda \times 1.9\,\lambda \times 2.1\,\lambda$) [43]. (c) Manufactured receiver chip with integrated receive antenna (*left*) and auxiliary transmit antenna (*right*) in K-band ($0.17\,\lambda \times 0.18\,\lambda$) [45].

2.2 Challenges in circuit-antenna integration

2.2.1 State-of-the-art design examples

Previous studies of PAIAA designs in various frequency bands are reported in [40]–[46]. Designs introduced in this section are in ascending order for frequencies.

Figure 2.3a and 2.3b present a C-band GaN-HEMT PAIAA design achieving a maximum output power of $38\,\mathrm{dBm}$ and a peak PAE of $59\,\%$, in which the PA and the antenna are interconnected through a harmonic tuning circuit[2] and an IMN [43]. Although this design has good thermal management capabilities, the integrated antenna size is rather bulky ($1.9\,\lambda \times 1.9\,\lambda \times 2.1\,\lambda$).

[2]The harmonic tuning circuit is used to shape the drain waveform of the second and third harmonics to enhance the efficiency and fundamental output power of PAs.

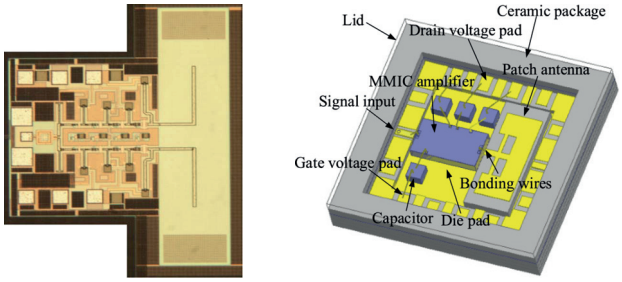

Figure 2.4: (a) A W-band transmitter RF front-end block composed of the PA and the antenna ($0.4\,\lambda \times 0.4\,\lambda$) [44]. (b) Illustration of an AIAiP ($0.8\,\lambda \times 0.8\,\lambda$) [46].

A monolithic 24-GHz receiver integrated with an on-chip folded dipole antenna was manufactured in a 0.8-μm SiGe HBT process. This design is compact in terms of wavelength ($0.17\,\lambda \times 0.18\,\lambda$), as shown in Figure 2.3c. However, the integrated on-chip radiator only has $-2\,\mathrm{dBi}$ gain [45].

Figure 2.4a shows a W-band PAIAA design in silicon technology [44]. The antenna size is $0.4\,\lambda \times 0.4\,\lambda$. However, its peak PAE is merely $6.4\,\%$, and the measured active antenna gain (G_{AIA}, *cf.* Section 1.7) is $9.4\,\mathrm{dB}$, where the dipole antenna gain is $-8.5\,\mathrm{dBi}$.

Song et al. presented a Ka-band AIA in package (AIAiP) [46]. The antenna is implemented on a PCB and integrated with an MMIC amplifier on the GaAs process. The antenna and the amplifier are assembled with packaging technology and interconnected by the wire-bond process, as shown in Figure 2.4b. The size of the AIAiP is $0.8\,\lambda \times 0.8\,\lambda$, and it demonstrated a total gain of $18.9\,\mathrm{dBi}$ at $35\,\mathrm{GHz}$; however, the efficiency and the gain of the PA are not documented.

Integrated solutions implemented in AoC and AiP are cost-effective at the higher end of mmWave frequencies, typically above $60\,\mathrm{GHz}$. At lower frequencies, on-chip implementation is challenging due to a relatively large chip area needed. Therefore, AoCs at frequencies below $60\,\mathrm{GHz}$ become expensive and may even not be manufacturable due to the restriction of the process. For instance, the maximum deliverable reticle size of the process can be in the order of $10\,\mathrm{mm} \times 10\,\mathrm{mm}$.

As mentioned in Section 1.4, other design challenges may occur depending on the implemented technology (e.g., AoC or AiP). These technology challenges and the solutions are outside the scope of this work and thus are not discussed.

2.2.2 Challenges of direct impedance matching for antenna-PA integration modules

One major design challenge in PAIAAs is to determine the optimal PA-antenna interface impedance. On the one hand, high-power PAs typically prefer a low optimal load resistance and an inductive load to resonate out the output capacitance for maximum efficiency and delivered power. However, the choice of substrate technology determines the breakdown voltage of the transistor, and the breakdown voltage bounds the optimal load resistance of the transistor[3]. On the other hand, the antenna input resistance is typically high for attaining high radiation efficiency, such as $50\,\Omega$ or $75\,\Omega$, which are the typical characteristic impedances of transmission lines. The optimum load impedance of the two sub-systems is profoundly distinct. Therefore it is improbable to find an arbitrary interface impedance that can attain the peak performance of both sub-systems. Hence, a trade-off study is required to determine the optimal interface impedance that can lead us to the targeted design goals.

Among the plethora of studies on PAIAAs, there is a lack of PA-antenna co-design methodology for achieving optimal AIA designs that account for both PA nonlinear behavior and antenna MC effects accurately. A summary table of the state-of-the-art PAIAA designs and their challenges are listed in Table 2.2. These examples indicate the common challenges as well as the challenges associated with the specific implementation solutions (e.g., AoC, AiP, or hybrid.)

Table 2.2: State-of-the-art PAIAA examples and the design challenges

Ref	Topology	Implement solutions	Freq [GHz]	Challenges
[40]	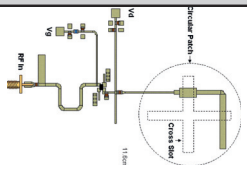	Hybrid, Conventional	2	Antenna element size not suitable for array applications ($> \lambda/2$)

Continued on next page

[3]Typical optimal load resistance of PA is around $18\,\Omega$ for GaN technology. It is around $5\,\Omega$ for CMOS technology.

Table 2.2: State-of-the-art PAIAA examples and the design challenges (continued)

Ref	Topology	Implement solutions	Freq [GHz]	Challenges
[8]	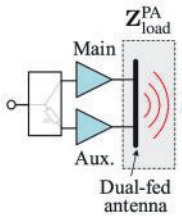	Hybrid, high integration	2.14	Antenna element size not suitable for array applications ($> \lambda/2$), challenging to precisely control the dual-fed to the Doherty PA
[37]	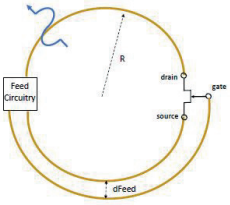	Hybrid, deep integration	3	Challenging to implement and troubleshoot, high risk of self-oscillation
[42]	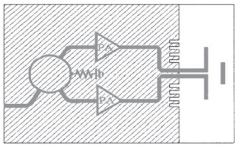	Hybrid, conventional	4.15	Antenna element size not suitable for array applications ($> \lambda/2$)
[43]	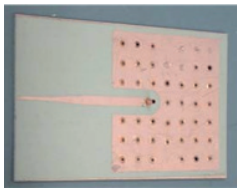	Hybrid, conventional	5.8	Antenna element size not suitable for array applications ($> \lambda/2$), not optimized via direct match, w/o co-design
[41]	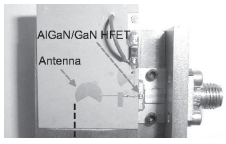	Hybrid, conventional	7.25	Antenna element size not suitable for array applications ($> \lambda/2$), narrowband ($<1\,\%$)

Continued on next page

Table 2.2: State-of-the-art PAIAA examples and the design challenges (continued)

Ref	Topology	Implement solutions	Freq [GHz]	Challenges
[45]	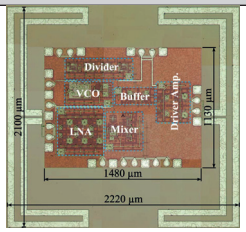	AoC, high integration	24	Low antenna gain ($-2\,\mathrm{dBi}$), narrowband ($<3\,\%$)
[47]	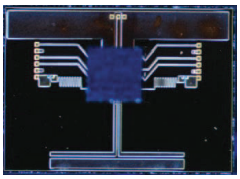	AoC, high integration	24	Low efficiencies (simulated PAE $< 25.6\%$, $\eta_{\mathrm{rad}} < 60\%$)
[46]	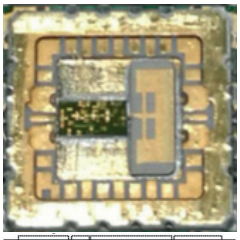	AiP, conventional	35	Antenna element size not suitable for array applications ($0.8\,\lambda \times 0.8\,\lambda$), Γ_{ant} effected by package size, not optimized via direct match, w/o co-design
[48]	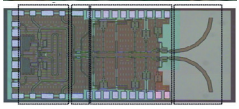	AoC, conventional	60	Low η_{ant}, not optimized via direct match, w/o co-design
[44]	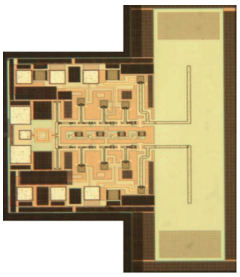	AoC, high integration	79	Low η_{ant} ($G_{\mathrm{ant}} = -8.5\,\mathrm{dBi}$)

2.2.3 Novelty of this thesis

The common challenges of the AIAs include, but not limited to: a) oversized form factor not suitable for array applications, b) inferior efficiencies (PAE and antenna radiation efficiency), c) not co-optimizing via direct impedance match (i.e., *high integration* concept), and d) conventional design methodology (circuit and antenna not designed and optimized jointly). The novelties of this thesis are:

I Proposed a preliminary design flow for AIAs in the mmWave frequency range.

II Presented a co-design methodology, where a combined EM circuit multiport analysis is utilized to co-optimize the integrated design, including taking into account the OTA coupling (antenna feedback) effects and the nonlinear behavior of active devices.

III Demonstrated an example of a relatively low-cost, compact, high-efficiency, and high-power integration antenna element design for active array systems by using the design flow and the methodology.

2.3 Multidisciplinary design approaches

2.3.1 Co-Design Flow

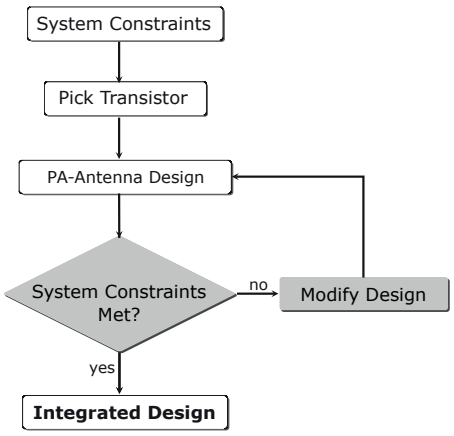

Figure 2.5: Preliminary co-design flow.

A multidisciplinary co-design strategy is needed to avoid (or minimize) the use of IMNs, which can potentially mitigate the insertion losses and enhance the efficiency and bandwidth by directly matching the antenna impedance to the optimal load impedance of the PA[4] rather than to 50-Ω. Figure 2.5 describes the iterative optimization process of the preliminarily proposed design flow. Regarding the PA design, our choice of the integration level at the initial stage is to limit ourselves to a transistor-on-chip and to design the remaining circuitry off-chip, including the radiating element. In the future, the integrated circuit (IC) design of the PA can be conducted in-house, and the distribution of on- and off-chip components of the AIA can be determined more optimally.

Choice of transistor The maximum available output power of semiconductor devices is intrinsically bounded by the breakdown voltage of the technologies [6]. III-V compounds such as Gallium Arsenide (GaAs) and fast-growing GaN materials are common design choices for mmWave ICs owing to their relatively high peak output power [6], [49], as shown in Figure 2.6a. Notwithstanding, III-V materials are more expensive than silicon-based technologies and offer limited flexibility in terms of complex integrated designs.

For these reasons and along with the targeted system constraints listed in Section 1.3, GaN-based IC technology looks most promising when it comes to a PAIAA co-design. Among the off-the-shelf transistors, Qorvo TGF2942 GaN HEMT [50] shows high-power and high-efficiency characteristics between $20\,\mathrm{GHz}$ to $30\,\mathrm{GHz}$, demonstrating appealing traits for PAIAA designs in this frequency range.

A Modelithics model [51] of the Qorvo HEMT is available in Advanced Design System (ADS) [52] for numerical analysis. The modeled I-V characteristics of the transistor can be used to determine the DC-bias point. The load-pull for maximum PAE at $20\,\mathrm{GHz}$ is presented in Figure 2.6b, which shows that the optimal load impedance has a relatively low resistance and a series inductance ($17 + \mathrm{j}46\Omega$) for a peak PAE of $56\,\%$. The low optimal load resistance of the PA complicates the antenna-PA direct matching because it requires an antenna with low radiation resistance.

The modeled maximum available gain of the transistor revealed that the PA is *conditionally stable* (*cf.* Section 1.7), as shown in Figure 2.7. An RLC (resistor, inductor, capacitor) stability circuit connected immediately to the gate of the transistor is needed to reach *unconditional stability* (*cf.* Section 1.7), as shown in Figure 2.8. A conjugate match at PA input was implemented to enhance the power gain.

[4] In this design example, the interface impedance is chosen to be the PA optimal load impedance.

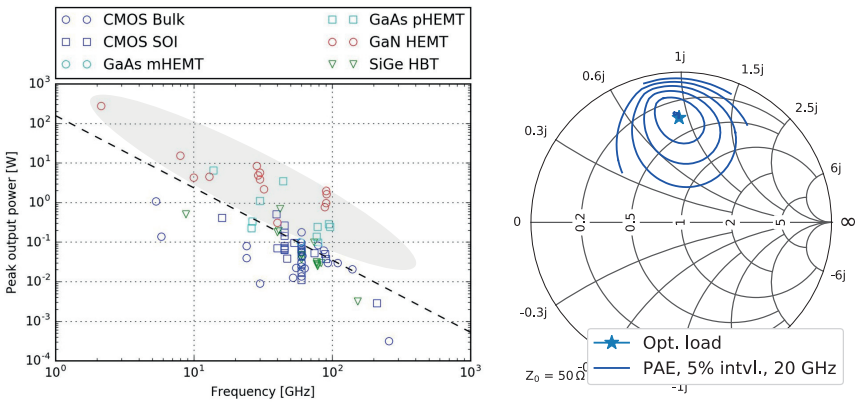

(a) (b)

Figure 2.6: (a) III-V materials are most promising for PAIAA co-design in mmWave frequency range due to its high peak output power [6]. (b) ADS modeled load-pull for maximum PAE of Qorvo TGF2942 HEMT [50]. Bias conditions: $V_{\mathrm{DS}} = 28\,\mathrm{V}$, $I_{\mathrm{DS}} = 40\,\mathrm{mA}$, bond wires excluded.

Choice of antenna element In the initial design, the interface impedance between the PA and antenna is set to be the optimal load impedance of the PA to achieve high PAE. The PA output must be matched to an antenna (a load) with a low radiation resistance and an inductive reactance. The inductance is desired to compensate for the capacitance at the transistor output. In the following design iterations, the antenna is selected to synthesize the aforementioned optimal load impedance; this obviates the need for an output IMN, which can potentially reduce the insertion and mismatch losses to enhance both the system efficiency and total radiated power.

Additionally, thermal management is a crucial issue in PA or PAIAA designs, especially for high-power amplifiers with inferior PAE that tend to dissipate much heat. The PCB-made antennas are cost-effective and thus suitable for mass production; however, these antennas suffer from inferior radiation efficiency due to the conductor and dielectric losses, and its feature of thermal management is limited. Metal-only antennas not only benefit from high radiation efficiencies but also can ease the thermal management issues as the antennas also serve as heatsinks to help remove the heat from the transistor.

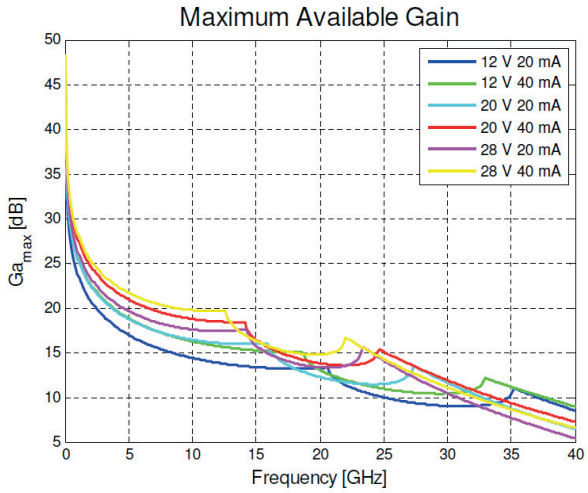

Figure 2.7: Modeled maximum available gain of Qorvo TGF2942 GaN HEMT at various bias points [50], which shows the transistor is conditionally stable.

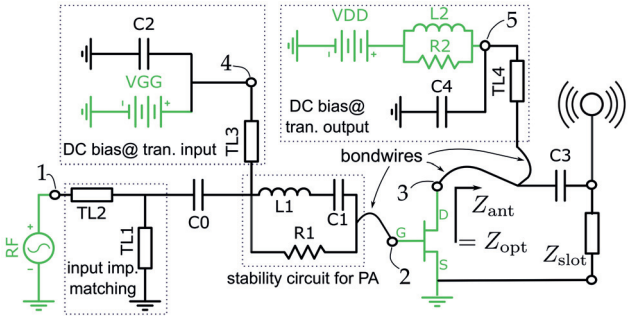

Figure 2.8: Schematic of the proposed PAIAA design providing a direct optimal impedance match to the PA to maximize efficiency while obviating the use of (a lossy) IMN. The transistor chip is integrated via a bond wire over the radiating slot. **Green** components were modeled in the circuit solver; black components were modeled in the full-wave EM solver.

Co-optimization The proposed PAIAA design was jointly optimized through a combined EM-circuit analysis approach (introduced in the following paragraph). The

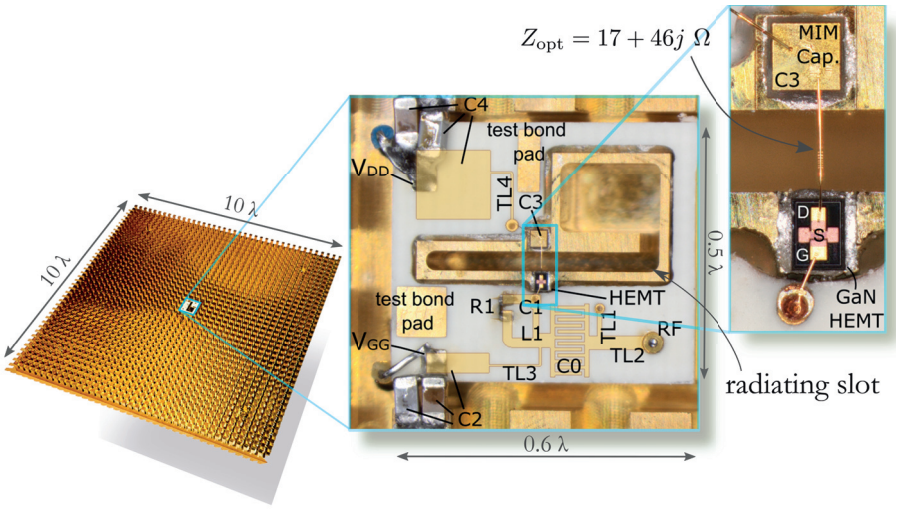

Figure 2.9: PAIAA element operating at 20 GHz center frequency. The parameters of the radiating slot are shown in Table 2.3 and Figure 2.12. The shown circuitry corresponds to the schematic in Figure 2.8, in which the translucent part is embedded in the middle layer of PCB laminate.

schematic of the PAIAA design is shown in Figure 2.8, in which the radiating element is directly integrated to the PA via a bond wire across the radiating slot, as shown in Figure 2.9, without using any IMNs to interconnect. The surrounding circuitry, including the DC-bias networks, the stability circuit, and the input IMN, is standard circuit blocks in amplifier designs.

Obviating the output IMN can make a more compact design. In conventional integration design such as in [43], an IMN is required to transform the impedance to 50 Ω and a harmonic circuit to boost the PA efficiency, as shown in Figure 2.3a. However, in the co-designed high integrated AIA proposed herein, both the IMN and the harmonic circuit can be realized within the antenna.

2.3.2 Harmonic termination

The peak efficiency and the fundamental output power of PAs are affected by the second and third harmonics drain waveform shaping [53], [54], of which the efficiency can be treated as a function of the second and third harmonic impedances.

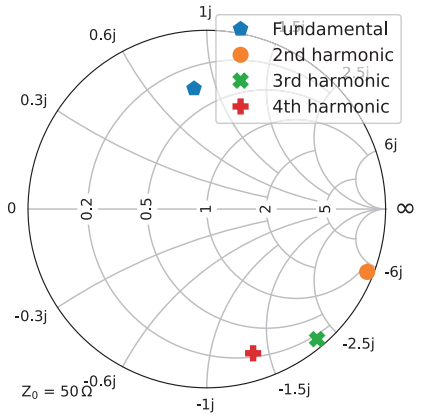

Figure 2.10: Modeled impedance of the radiating slot at the fundamental frequency (20 GHz) and the second, third, and fourth harmonics.

In general, the peak efficiency requires harmonic short or open terminations at the amplifier output to generate pure sinusoidal voltage and current waveforms [53]. In this work, the antenna impedance at the second harmonic shows $|\Gamma_D(2f_o)|$ [5] ≥ 0.96 ($\mathcal{S}_{11}^{2f_o} \simeq -0.3\,\mathrm{dB}$) and $\angle\Gamma_D(2f_o)$ within 22.5° of an open circuit; at the third harmonic the antenna impedance is $|\Gamma_D(3f_o)| \geq 0.95$ ($\mathcal{S}_{11}^{3f_o} \simeq -0.4\,\mathrm{dB}$) and $\angle\Gamma_D(3f_o)$ within 50° of an open circuit, as shown in Figure 2.10. Peak efficiency of $49.5\,\%$ can be achieved theoretically with this harmonic termination. It is possible to expect a $3\,\%$ drop in efficiency without any proper harmonic termination. In a less linear PA, the efficiency reduction can be even worse.

2.3.3 Combined EM-circuit analysis

Figure 2.8 shows that the RF/DC sources and the transistor model are numerically analyzed in ADS while the remainder, i.e., the passive components and the radiating slot, is analyzed in the combined EM-circuit solver. The nonlinear effects of the active components cannot be analyzed in EM simulators, and therefore, the combined EM-circuit solver is required to take account of these nonlinear effects. Nonlinear effects are essential, which shall not be ignored because they can impact the system performance if not handled carefully. For instance, the third-order intercept point

[5] $\Gamma_D(f_o)$: The reflection coefficient seen looking toward the radiating slot at frequency f_o.

(TOI) indicates the vulnerability to intermodulation distortion (IMD) of the system when two or more signals are fed to the nonlinear device. By using the combined EM-circuit analysis, one can ensure the TOI is sufficiently higher than the P1dB to prevent the system from suffering IMD.

Typically, there is only one port per antenna element in passive antennas to represent the excitation port. For PAIAA designs, multiple ports per antenna are required to analyze and co-optimize the radiating structure and the integrated active device jointly. It is indispensable to have an accurate analysis of the coupling mechanism between all the ports since, as the element is used in an antenna array, couplings may exist between these ports. The coupling mechanism of AIA arrays is more complicated than passive antenna arrays due to that the reflected or coupled waves can alter the PA load impedance and thereby the system characteristics or give rise to undesired feedback, possibly affecting the system stability [7].

As can be seen in Figure 2.8 and 2.11, the proposed PAIAA is a five-port circuit-antenna integrated design. The combined EM-circuit solver is interconnected and mapped by five single-mode ports between the circuit schematic and the EM model, as shown in Figure 2.8 and Figure 2.11, respectively. Multiple iterations are required to realize a co-optimized PAIAA design, such as adjusting the DC-bias for PA to improve the PAE or power and modifying the antenna to increase its radiation efficiency without compromising the PAE.

The PA presented in [44] was assumed as a metallic plate in the EM solver, thereby neglecting the dielectric effect and approximating the OTA coupling behavior in the vicinity of the transition between the PA and the dipole antenna. In this work, the substrate, the bonding pads, and the metallic ground (*source*) of the transistor chip are included in the EM model. Besides, the bond wires are also included in the numerical model to excite the radiating element (from the drain pad across the radiating slot) and to interconnect the other circuitry components, as shown in Figure 2.9.

2.4 Power amplifier-integrated active antenna element design example

The proposed PAIAA element consists of a Rogers RO4350B multilayer PCB laminate for the PA circuitry and a metallic radiating structure. For a direct PA-antenna impedance match, a cavity-backed slot antenna was selected. Furthermore, a stub ($W_3 \times L_3 \times H_2$) was appended to the extremity of the slot ($W_4 \times L_2 \times H_2$) to alter the radiation impedance, as shown in Figure 2.12. The impedance tuning parame-

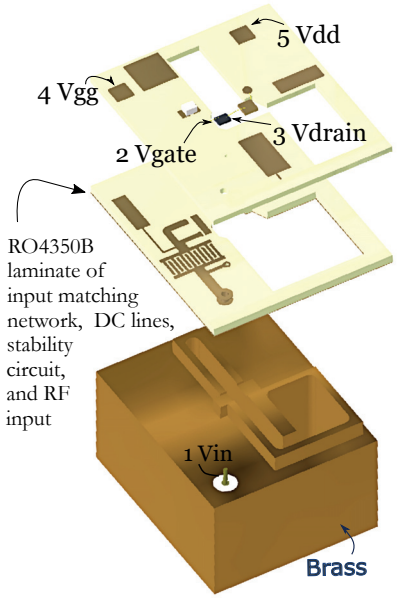

Figure 2.11: Five ports of the PAIAA model used in the co-design are denoted: $V_{in}, V_{gate}, V_{drain}, V_{gg}, V_{dd}$, which correspond to the ports in Figure 2.8.

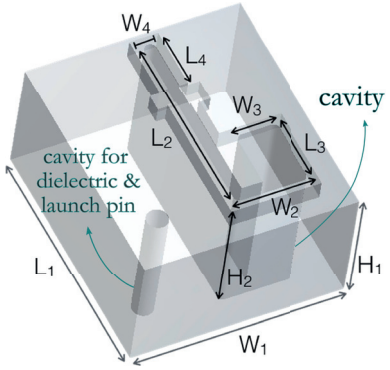

Figure 2.12: The geometry of the proposed PAIAA design. The design parameters are listed in Table 2.3.

ters are $H_2, L_2, L_3, L_4, W_2, W_3, W_4$, and their values are listed in Table 2.3, where $L_1 \times W_1 \times H_1$ indicates the integrated antenna element dimensions.

Table 2.3: Geometrical parameters (unit: mm).

L_1	L_2	L_3	L_4	W_1	W_2	W_3	W_4	H_1	H_2
9.1	7.3	3.1	3.2	7.5	3.4	2.2	0.6	5.4	5.0

2.5 Measurement and calibration setup

An illustration of the measurement setup and the reference planes is presented in Figure 2.14. The PAIAA was connected to an Agilent E8363B PNA network analyzer, and DC-powered by a Rohde & Schwarz HMP4040 power supply. A pre-amplifier was used to increase the input power to the desired range ($-10\,\mathrm{dBm}$ to $25\,\mathrm{dBm}$). The reference plane for the received power ($P_{\text{rx,pna}}$), the input power ($P_{\text{tx,pna}}$), and the power accepted (P_{acc}) and radiated (P_{out}) by the DUT are denoted in Figure 2.14.

The characterization of the PAIAA was conducted in the anechoic chamber, as shown in Figure 2.13, achieved a maximum active antenna gain of $15\,\mathrm{dBi}$ with a $50\,\%$ peak total efficiency (PAE $\cdot\, \eta_{\text{rad}}$, ref. plane E). Different from the conventional integrated designs, where the PA and the antenna can be designed and characterized independently, the transistor chip is directly integrated to the antenna forming the PAIAA—device under test (DUT), as shown in Figure 2.9. Consequently, the antenna and PA of the DUT need to be characterized jointly, which increases the measurement complexity.

The presented characterization procedure consists of two measurement steps.

Step 1: Conduct the measurement with a standard-gain horn antenna (the receiving antenna) connected to port 2 of the PNA and a reference antenna (with known gain $G_{\text{ref.ant}}$) connected to the pre-amplifier and then to port 1 of the PNA. This is a calibration step to find the "path gain" G_{path}, which includes all gains and losses but excludes the known reference antenna gain ($G_{\text{ref.ant}}$, defined between ref. plane B and C).

$$G_{\text{path}} = |S_{21}|^2_{\text{ref}} / G_{\text{ref.ant}} \,, \tag{2.1}$$

where $|S_{21}|^2_{\text{ref}}$ is the measured transmission coefficient between the PNA ports (reference plane A and D).

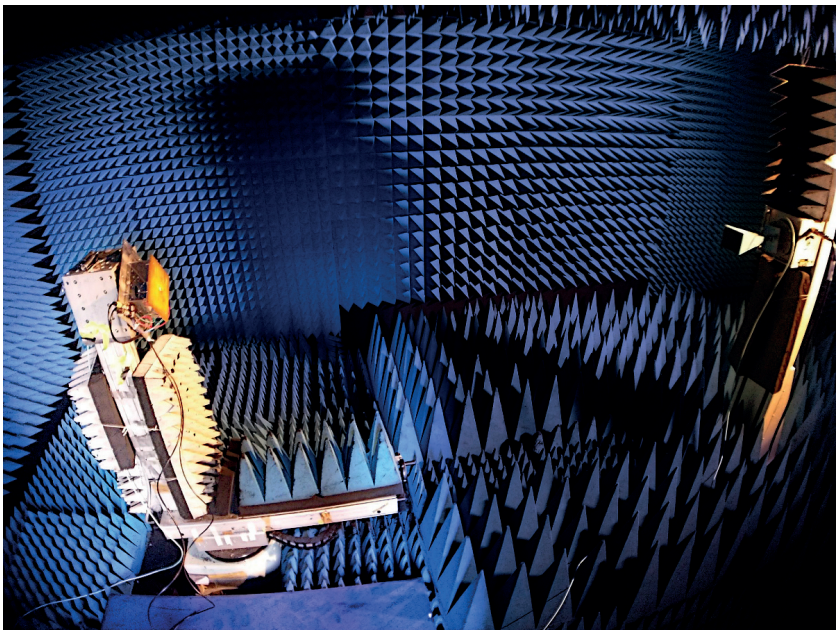

Figure 2.13: OTA characterization in the anechoic chamber. The DUT (the transmitting antenna—PAIAA) is on the left, and a standard-gain horn receiving antenna is on the right, performing the line-of-sight characterization.

Step 2: Figure 2.14b shows the setup of this step. The reference antenna is replaced with the DUT. The active antenna gain ($G_{\text{AIA}} = G_{\text{P}} G_{\text{ant}}$) of the DUT is obtained from

$$G_{\text{P}} \eta_{\text{rad}} D_{\text{ant}} = |S_{21}|^2 / G_{\text{path}} \, , \tag{2.2}$$

where G_{P} is the PA power gain, η_{rad} is the antenna radiation efficiency, D_{ant} is the antenna directivity, which is determined by measuring the radiation pattern over the whole angular space, and $|S_{21}|^2$ is the measured transmission coefficient from PNA port 1 ($P_{\text{tx,pna}}$, ref. plane A) to port 2 ($P_{\text{rx,pna}}$, ref. plane D). Hence, the PA power gain, together with the antenna radiation efficiency, is obtained by

$$G_{\text{P}} \eta_{\text{rad}} = |S_{21}|^2 / (G_{\text{path}} D_{\text{ant}}). \tag{2.3}$$

For the efficiencies, the value of the DC power (P_{DC}) and the radiated power (P_{out}) at

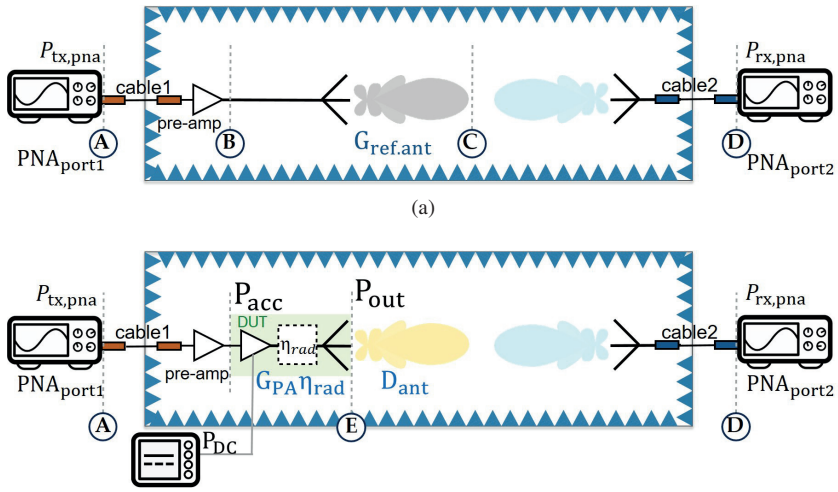

Figure 2.14: (a) Calibration with the reference antenna in the anechoic chamber. (b) OTA characterization of the proposed PAIAA in the anechoic chamber.

the reference plane E is required. While P_{DC} is obtained by monitoring the DC power supply, P_{out} is calculated from knowing the available power at PNA port 1 ($P_{tx,pna}$), the cable losses, the pre-amplifier gain, and the PA gain and antenna radiation efficiency.

2.5.1 Results

The PA transducer gain and antenna radiation efficiency $G_{PA}\eta_{rad} = P_{out}/P_{acc}$, is plotted in Figure 2.15a. An average PA transducer gain (including the antenna radiation efficiency) of $8\,dB$ is observed from $19.5\,GHz$ to $20\,GHz$. The gain at $20\,GHz$ is about $9\,dB$, showing a reasonable agreement with the combined EM-circuit numerical result, although compressed earlier than expected. The simulation result confirmed that the PA could compress before reaching the saturated power[6] if the load impedance is drifted away from the optimal load impedance. The PA gain (including the antenna radiation efficiency) is plotted against frequency for two available input power ($P_{acc} = 15, 20$ [dBm]), as shown in Figure 2.16a. In the latter scenario, it starts to show gain compression due to the output power is approaching the saturated

[6]maximum output power of a PA

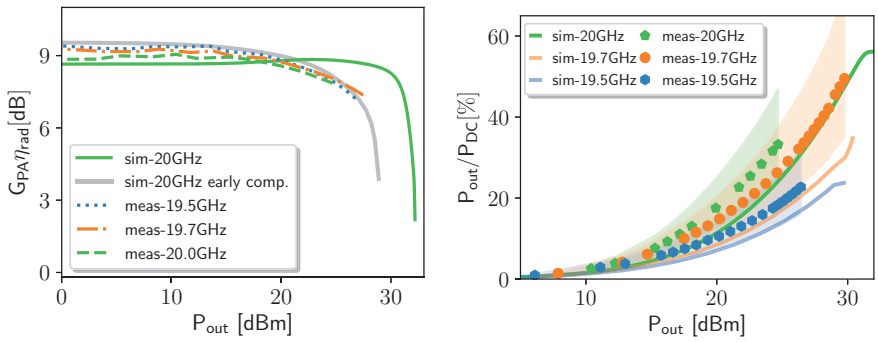

(a) (b)

Figure 2.15: (a) The PA transducer gain including the antenna radiation efficiency at reference plane E (*cf.* Figure 2.14b), and (b) the efficiency and measurement uncertainty (± 1.5 dB, colored shadows) at the fundamental frequencies versus RF output power.

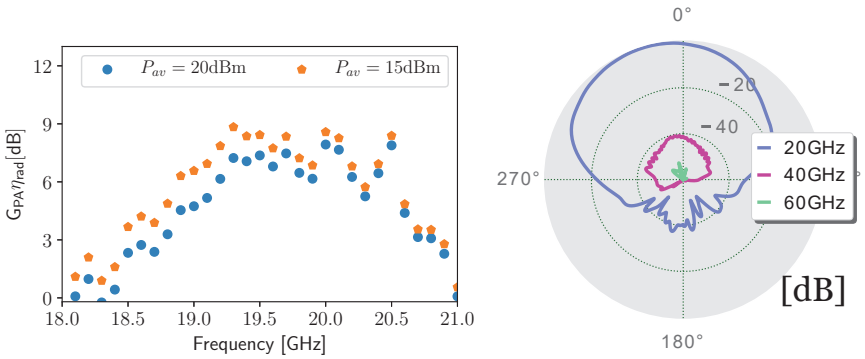

(a) (b)

Figure 2.16: (a) The PA transducer gain including the antenna radiation efficiency at reference plane E (*cf.* Figure 2.14b) versus frequencies for two available input power: $P_{acc} = 15$ dBm (orange pentagon), and $P_{acc} = 20$ dBm (blue circle). The PA gain shows signs of compression in the latter case. (b) Numerical results of the second and third harmonics radiation compared to the fundamental frequency (20 GHz).

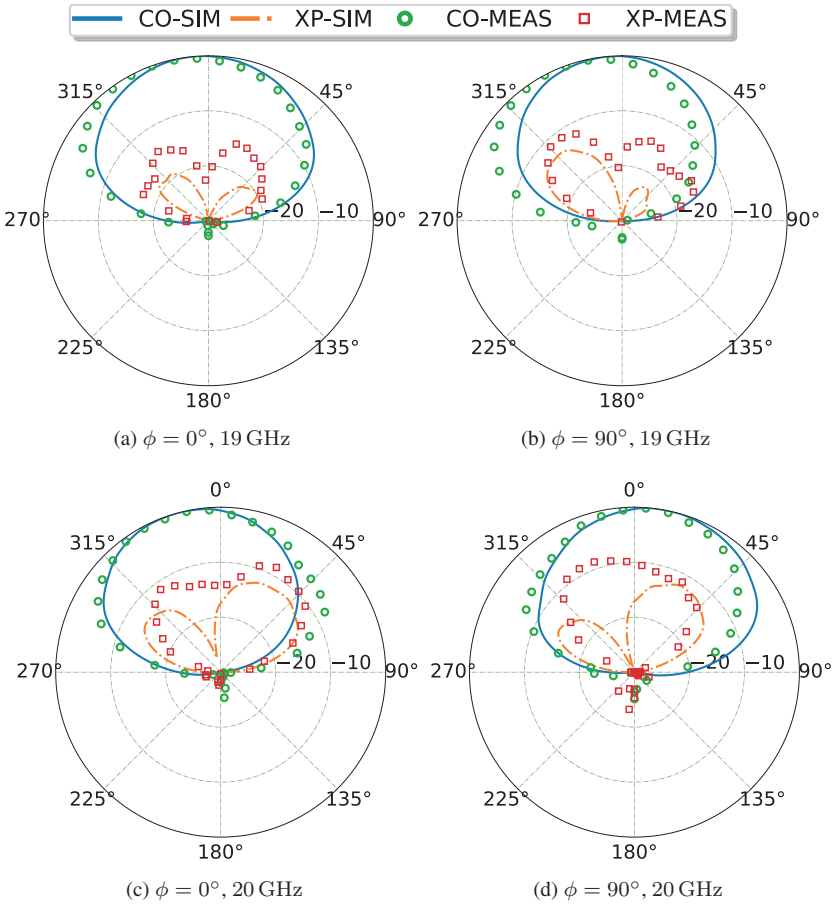

(a) $\phi = 0°$, 19 GHz (b) $\phi = 90°$, 19 GHz

(c) $\phi = 0°$, 20 GHz (d) $\phi = 90°$, 20 GHz

Figure 2.17: Normalized radiation pattern at 19 GHz on (a) $\phi = 0°$ and (b) $\phi = 90°$, and at 20 GHz on (c) $\phi = 0°$ and (d) $\phi = 90°$.

output power of the PA.

The measured efficiency is shown in Figure 2.15b, in which the measurement uncertainty of ± 1.5 dB is also depicted. The uncertainties are mainly caused by the non-ideal measurement environment and setup, such as the probe misalignment, reflection in the chamber, and tolerances on the calculated path loss and reference antenna gain. Note that the frequency shift in the measurement results is believed due to manufac-

turing and assembly tolerances. The simulated radiation patterns of the second and third harmonics are shown in Figure. 2.16b, in which the harmonic radiation is at least $40\,\mathrm{dB}$ lower than at fundamental. The measured radiation patterns are shown in Figure 2.17, which demonstrate good agreements with the numerical results. A comparison with the state-of-the-art PAIAA designs is presented in Table 2.4.

2.6 Conclusion

A comparison of our design with state-of-the-art PAIAA design shows that the efficiency and the equivalent isotropically radiated power (EIRP) are comparable to the PAIAA design in C-band [43], yet with a considerably smaller electrical size and at much higher operating frequencies. The proposed design has demonstrated that a PAIAA with high peak efficiency ($49.5\,\%$ at $19.7\,\mathrm{GHz}$) and high output power ($28\,\mathrm{dBm}$) can be achieved by direct integration in conjunction with the proposed antenna-PA co-optimization methodology. By using a metal-only antenna, it is expected that the thermal dissipation problem to be alleviated. The proposed PAIAA is compact ($0.6\,\lambda \times 0.5\,\lambda$) and suitable to be applied in actively beamformed antenna arrays. The main directions for improvement are:

- to increase the frequency bandwidth,
- to realize in-house MMIC PAs for much compact PAIAA designs,
- to scale up the design to arrays.

Table 2.4: Performance comparison of the state-of-the-art PAIAAs.

	No OIMN*	Thermal handling	Transistor Technology	Frequency	$P_{1dB,out}$	EIRP	PAE peak	Dimensions $L \times W \times H$ [λ^3]
[40]	✓	poor	pHEMT	2 GHz	21.7 dBm	NA	>60 %	$0.6 \times 0.8 \times$ NA
[42]		poor	GaAs	4.15 GHz	28.2 dBm	NA	60.9 %	NA
[43]		great†	GaN HEMT	5.8 GHz	38 dBm	44.6 dBm	59.93 %	$1.9 \times 1.9 \times 2.1$
[41]	✓	poor	AlGaN/GaN	7.25 GHz	30.3 dBm	NA	42 %	NA
[45]	✓	poor	SiGe HBT	24 GHz	5.6 dBm	4.6 dBm	N/A	$0.2 \times 0.1 \times$ N/A
[47]	✓	poor	0.18 µm CMOS	24 GHz	N/A	N/A	25.6 %	$0.3 \times 0.2 \times$ N/A
[46]		poor	GaAs pHEMT	35 GHz	N/A	N/A	N/A	$0.8 \times 0.8 \times$ N/A
[48]		poor	BiCMOS	60 GHz	12.8 dBm	9.5 dBm	N/A	$0.2 \times 0.2 \times$ N/A
[44]	✓	poor	BiCMOS	79 GHz	19 dBm	3 dBm	11 %‡	$0.4 \times 0.4 \times$ N/A
This work	✓	good	GaN HEMT	20 GHz	24.7 dBm	30.7 dBm	34.8 %	$0.6 \times 0.5 \times 0.3$

*output impedance matching network †installed on a Peltier unit ‡simulated results

CHAPTER 3

Integrated Array Antenna

In this chapter, a summary of the MC study is given, in which we have proposed a scattering parameters (S-matrix) re-normalization procedure to help with the investigation of the interaction effects in integrated array antennas.

3.1 Mutual coupling

An important observation from the recent years of research in the area of modern array antenna systems is that understanding the OTA coupling (antenna crosstalk) effects in integrated circuitry and the nonlinear behavior of PAs (active components) has a significant impact on the overall system performance. For instance, the linearity, efficiency, gain, output power, and the stability of the PA can deteriorate sharply if the antenna element MC effects are not considered during the design process. Even at the single-element level, the radiation of the antenna element may couple back over-the-air to the input of the PA circuitry [55]. On the other hand, one can exploit array MC effects to increase the beam scanning range and frequency bandwidth [56]. Hence, taking account of and understanding the MC effects in AIA arrays are essential. An overview of the design challenges of active beamforming antenna arrays was presented in [7]. The paper discussed that the overall system performance could

be substantially affected by MC effects, and therefore trade-offs are required in the antenna design process.

A combined EM-circuit *multiport* analysis was proposed (*cf.* Section 2.3.3) to deal with these design challenges. In this respect, arrays of such AIA elements are more complex to characterize in terms of antenna MC effects than the conventional arrays, i.e., passive antenna arrays or active antenna arrays with a single port reference impedance per element [57]. This complexity comes from the fact that a common approach of using standard 50-Ω normalized S-matrix for evaluating coupled port powers is no longer representative whenever the ports are terminated with impedances different from 50-Ohm. In that case, the S-matrix does not directly represent the actual power-wave coupling and reflection coefficients, although these models are mathematically correct.

Presently, there are a plethora of studies conducted on antenna MC. Craeye et al. conducted a comprehensive review of antenna array MC analysis methods to model these coupling effects [57]. Many works are mostly for passive antenna arrays or active antenna arrays of assuming a single port reference impedance Z_0. The MC effects for active receivers were discussed in [58]–[63], in which both analytical and numerical models were proposed and experimentally verified. In those papers, the system receiving sensitivity was shown to be affected by the noise at the receiver inputs that partly couples and re-enters the system via the mutually coupled antenna elements.

In the next section, we show that the S-matrix must be properly re-normalized to provide insights in the actual MC of power waves in integrated active transmitting antenna arrays, including the isolation level between the *drain* port (output) and the *gate* port (input) of the transistor. This re-normalized procedure can help improve the overall system performance and make essential design trade-offs (e.g., the interplay between the PA and antenna design aspects).

3.2 S-matrix re-normalization

To extract useful physical information from the S-matrix ($\mathcal{S}$) of the multiport PA-IAA with port reference impedances ($\mathcal{Z}_i$), $\mathcal{S}$ is re-normalized with port reference impedances ($\mathcal{Z}_i'$) chosen to be equal to the actual port terminations (i.e., the output impedances of the interconnected circuits) to arrive at $\mathcal{S}'$. To this end, we follow the normalization procedure, as described in [64]. The re-normalized S-matrix $\mathcal{S}'$ are generally different from the standard 50-Ω $\mathcal{S}$ and can be expressed in terms of $\mathcal{S}$ as

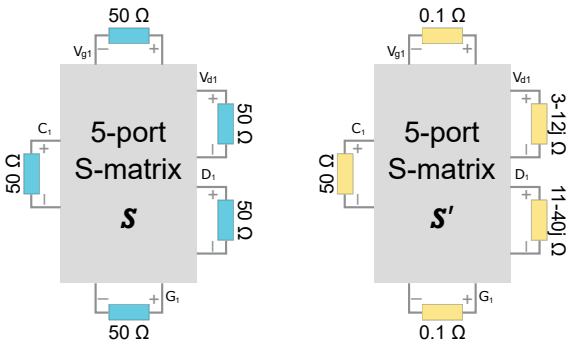

(a) $\mathcal{S}$ (b) $\mathcal{S}'$

Figure 3.1: Diagram of the scattering matrix of the 5-port PAIAA (a) with standard 50-Ω as the port reference impedance and (b) with reference impedances $\mathcal{Z}_i'$ for an isolated antenna element as shown in Figure 2.9.

$$\mathcal{S}' = \mathcal{A}^{-1}(\mathcal{S} - \Gamma^{\mathrm{H}})(\mathcal{I} - \Gamma\mathcal{S})^{-1}\mathcal{A}^{\mathrm{H}}\,, \tag{3.1}$$

where the superscript H denotes conjugate transpose, and Γ and $\mathcal{A}$ are diagonal matrices with their i-th diagonal components being r_i and $(1-r_i^*)\sqrt{|1-r_i r_i^*|}/|1-r_i|$, respectively; r_i is the power wave reflection coefficient of $\mathcal{Z}_i'$ with respect to $\mathcal{Z}_i^*$, i.e.

$$r_i = \frac{\mathcal{Z}_i' - \mathcal{Z}_i}{\mathcal{Z}_i' + \mathcal{Z}_i^*}.$$

Figure 3.1b illustrates the concept of the re-normalized S-matrix $\mathcal{S}'$ with port reference impedance $\mathcal{Z}_i'$ $(i = 1, 2, \ldots, 5)$, which provides a more accurate depiction of the actual power-wave coupling behavior of the PAIAA, as shown in Figure 3.2, in terms of port terminations as opposed to using the standard 50-Ω S-matrix, as shown in Figure 3.1a.

More specifically, the set of modified port reference impedances $\{\mathcal{Z}_i'\}$ is chosen as follows. Port 1 of the combined EM-circuit PAIAA design (*cf.* Section 2.4) connected to the RF input source, port 2 and port 3 connected to the drain (output) and gate

$\mathcal{A}^H$: the conjugate transpose of matrix $\mathcal{A}$

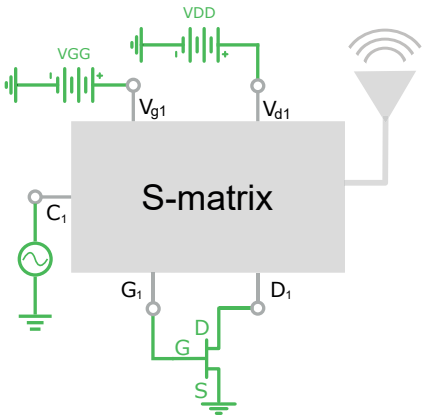

Figure 3.2: Schematic of the scattering matrix of the five-port PAIAA implemented in the EM-circuit co-design [55].

(input) of the transistor, and port 4 and 5 connected to a DC power supply at the drain and gate sides, respectively. The newly chosen port reference impedances of port 2 and 3 have to represent the output and input impedance of the Qorvo HEMT (modeled result from the Modelithics small-signal model was used herein), and the DC ports (port 4 and 5) have to be (near-)short-circuited while the reference impedance at port 1 remains $50\,\Omega$.

Intra-element MC

Intra-element MC is defined as the interactive effects between the ports at the same antenna element.

Inter-element MC

Inter-element MC is defined as the interactive effects between the ports at different array antenna elements.

The magnitude of the re-normalized S-matrix elements (dB($|\mathcal{S}'_{ij}|$)) at $20\,\mathrm{GHz}$ of an isolated 5-port PAIAA element is presented in Figure 3.3b, in which the diagonal components represent the reflection coefficient at each port. The notations of the

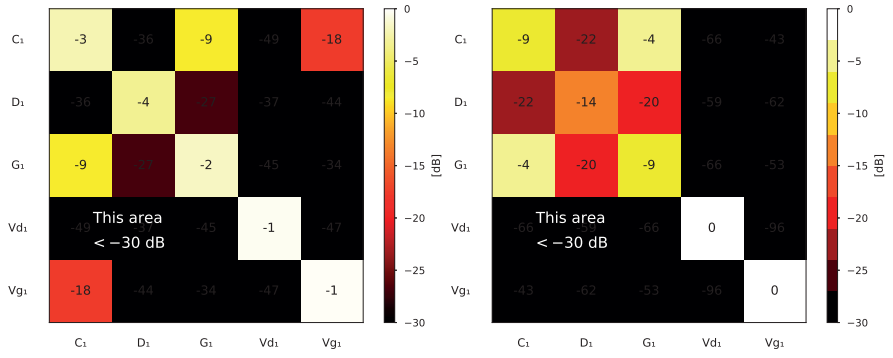

(a) (b)

Figure 3.3: Magnitude of the S-matrix with (a) $50\,\Omega$ as the port reference impedance (*cf.* Figure 3.1a) and (b) with port reference impedances $\mathcal{Z}_i'$ (*cf.* Figure 3.1b) for an isolated PAIAA element as shown in Figure 2.9.

antenna ports are as follows:

- C_m – *coaxial* port of the AIA element,
- D_m – *drain* port of the transistor,
- G_m – *gate* port of the transistor,
- V_{dm} – dc at the drain side of the PA,
- V_{gm} – dc at the gate side of the PA,

where m indicates the m-th element of the antenna array. For instance, element $(\mathrm{C}_1, \mathrm{C}_1)$ in Figure 3.3b represents $\mathrm{dB}(|\mathcal{S}'_{\mathrm{C}_1\mathrm{C}_1}|)$; i.e., the reflection coefficient at the input port of the first antenna element, which is $-9\,\mathrm{dB}$ in this case.

The passive antenna S-matrix $\mathcal{S}'_{ij}$ *de facto* describes the inter-ports MC effects in the absence of PA amplification (active effects). In Figure 3.3b, $\mathrm{dB}|\mathcal{S}'_{\mathrm{D}_1\mathrm{G}_1}|$ shows no amplification between port 2 *drain* and port 3 *gate*, which is generally not the case for transistors in amplifier networks. $\mathrm{dB}|\mathcal{S}'_{\mathrm{D}_1\mathrm{G}_1}|) = -20\,\mathrm{dB}$ shows that the OTA interaction effects between the two ports in the absence of transistor amplification are relatively weak. Similarly, $\mathrm{dB}|\mathcal{S}'_{\mathrm{D}_1\mathrm{C}_1}|$ shows that the OTA interactive effects between port 2 *drain* and port 1 *coaxial* in the absence of transistor amplification is $-22\,\mathrm{dB}$;

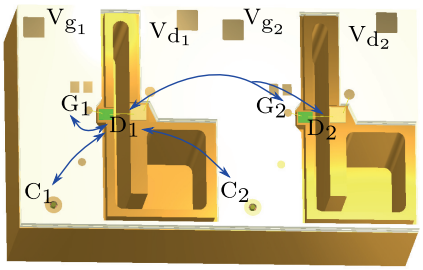

Figure 3.4: An illustration of potential interactive effects between the various ports of the multiport PAIAA elements in a 2×1 array.

this can be seen as sufficient isolation between the input and output of the amplifier provided that the power gain of the amplifier remains lower than this isolation by a sufficient margin. Further, $\mathrm{dB}|\mathcal{S}'_{\mathrm{D}_1\mathrm{D}_1}| \neq -\infty$ shows the reflection coefficient at port 2 *drain*. This finite value is not due to poor impedance matching at the port but because the antenna impedance is not conjugate-matched to the output impedance of the PA. As mentioned in [55], the interface impedance was chosen to maximize the PAE per the load-pull of the transistor, of which the loading condition is generally different from a conjugate match. $\mathrm{dB}|\mathcal{S}'_{\mathrm{D}_1\mathrm{D}_1}| = -14\,\mathrm{dB}$ suggests that a decent power gain can be obtained before the P1dB[1] because a conjugate match at PA output is required for maximum power gain. As mentioned before, the two DC ports $\mathrm{v}_{\mathrm{d}m}$, and $\mathrm{v}_{\mathrm{g}m}$ should represent (near-)short circuits, which explains the (near-)complete reflections at these ports resulting in the shown diagonal terms.

This re-normalization technique can also be applied to multiport PAIAA arrays. Suppose two elements are used in a linear array, as shown in Figure 3.4, the 50-Ω S-matrix shown in Figure 3.5a is now a 10×10 matrix, owing to that each element comprises 5 ports. The 10×10 S-matrix was subsequently re-normalized with port reference impedances $\mathcal{Z}'_i$ by using Eq. 3.1, as shown in Figure 3.5b. The re-normalization is required because the standard 50-Ω S-matrix provides limited to no immediate information on the actual power coupling coefficients between those ports. In the array scenario, the OTA coupling effects not only exist between the ports within the same element (*intra-element MC*) but can also occur between the ports located on different elements (*inter-element MC*). Among them, the coupling between port D_1 (port *drain*

[1] P1dB: The $1\,\mathrm{dB}$ compression point is the output power level at which the gain decreases 1 dB from its constant value.

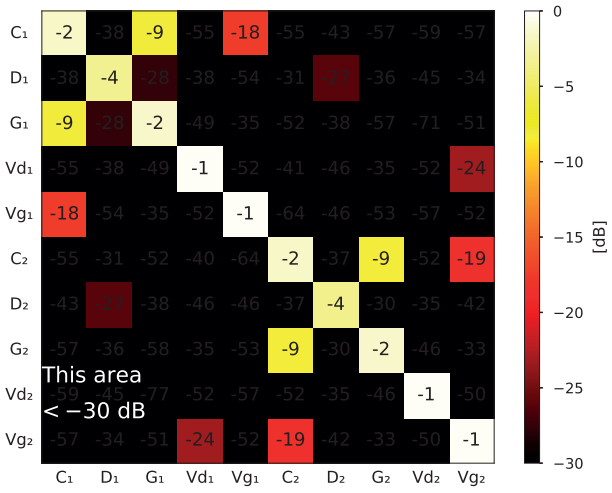

(a)

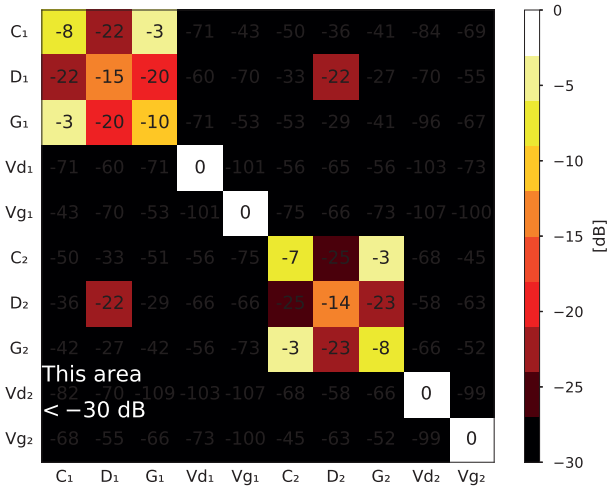

(b)

Figure 3.5: Magnitude of the S-matrix with (a) $50\,\Omega$ as the port reference impedance and (b) with port reference impedances $\mathcal{Z}_i'$ for 2×1 linear PAIAA array as shown in Figure 3.4.

at the first element) and port D_2 (port *drain* at the second element) shows the strongest inter-element coupling effect as these ports are used to excite the radiating slots and are thus closely related to the over-the-air slot-to-slot coupling in the array.

3.3 Summary

The standard 50-Ω S-matrix commonly used for analyzing antenna MC parameters is not fully representative of quantifying intra-element nor inter-element MC effects of power waves in highly integrated transmitting antenna arrays. In this chapter, an S-matrix re-normalization procedure is proposed that assumes the port reference impedances to be equal to the actual port terminations or the output impedance of the driving sources. This technique provides an insightful interpretation of the mutual coupling coefficients of power waves in integrated array antennas, of which the analysis is performed in the absence of transistor amplification (i.e., we set $S_{21}^{\mathrm{PA}} = S_{12}^{\mathrm{PA}} = 0$).

When applying the re-normalization technique to characterize an array of two elements, the critical findings on mutual coupling are:

- The intra-element OTA coupling between the drain port and the corresponding gate port is $< -20\,\mathrm{dB}$. The isolation level between the amplifier output and input is an essential index in PA design when it comes to, e.g., circuit stability.
- The inter-element OTA coupling from the drain port of the first element to the drain port of the second element is the strongest inter-element coupling, which is expected because these ports are employed to excite the radiating slots.
- The reflection coefficient at the drain port is not approaching $-\infty$. This is not due to a poor antenna impedance match to the PA output. In fact, the interface impedance was chosen to maximize the PAE, which is typically different from a conjugate match at the PA output. Yet, $\mathrm{dB}|\mathcal{S}'_{\mathrm{D}_1\mathrm{D}_1}| = -14\,\mathrm{dB}$ suggests that a decent power gain can be attained since a conjugate match is needed for maximum power gain.

CHAPTER 4

Summary of Included Papers

This chapter provides a summary of the included papers.

4.1 Paper A

Wan-Chun Liao, Rob Maaskant, Thomas Emanuelsson, Martin Johansson, Anders Höök, Johan Wettergren, Michael Dieudonne, Marianna Ivashina
A Ka-Band Active Integrated Antenna for 5G Applications: Initial Design Flow
Published in IEEE 2nd URSI Atlantic Radio Science Meeting (AT-RASC),
May 2018.
 DOI: 10.23919/URSI-AT-RASC.2018.8471330 .

Due to the lack of accurate and suitable AIA co-design approaches in the mmWave range, a preliminary interdisciplinary co-optimization methodology is proposed in this paper. It introduces the co-design procedure and how a customized interface impedance between the active devices and antenna can be determined to attain the optimal performance.

4.2 Paper B

Wan-Chun Liao, Rob Maaskant, Thomas Emanuelsson, Vessen Vassilev, Oleg Iupikov, Marianna Ivashina
A Directly Matched PA-Integrated K-band Antenna for Efficient mm-Wave High-Power Generation
Published in IEEE Antennas and Wireless Propagation Letters,
vol. 18, no. 11, pp. 2389–2393, Nov. 2019.
 DOI: 10.1109/LAWP.2019.2937235 .

A design example of a K-band GaN-based power amplifier integrated active antenna is presented in this paper. The PA-antenna was co-optimized through the EM-circuit co-design methodology proposed herein, and the direct impedance match with the optimal PA load impedance was applied to enhance the system efficiency. A maximum measured active antenna gain of $15\,\mathrm{dBi}$ and a peak efficiency of $49.5\,\%$ are reported.

4.3 Paper C

Wan-Chun Liao, Rob Maaskant, Thomas Emanuelsson, Artem Vilenskiy, and Marianna Ivashina,
Antenna Mutual Coupling Effects in Highly Integrated Transmitter Arrays
Accepted in Proceeding 14th European Conference on Antennas and Propagation (EuCAP), Copenhagen, Denmark, Apr. 2020.
 DOI: xx.xxxx .

In this paper, a scattering-parameter re-normalization procedure is presented. It describes how to re-normalize a standard 50-Ω scattering parameters with a customized set of port reference impedance and how the re-normalized parameters can be exploited to characterize the intra-element and inter-element MC effects on the level of a single element and an array.

CHAPTER 5

Concluding Remarks and Future Work

5.1 Conclusion

To develop new integration solutions for mmWave antenna arrays for various types of 5G applications, several objectives need to be met before reaching this goal. In this thesis, we have proposed a multidisciplinary co-design flow and methodology for integrated circuit-antenna modules, which can account for not only the interactive effects between the active devices and the radiating element but also for the nonlinear behavior of the active components. These effects can jeopardize the system performance if not treated carefully.

A design example of a K-band efficient high-power GaN-based PAIAA element was demonstrated in Chapter 2 as a proof of concept of the multidisciplinary co-optimization methodology. Direct integration is adopted in the design of the highly integrated PA-antenna module, in which a measured active antenna gain of $15\,\mathrm{dBi}$ and peak total efficiency of $49.5\,\%$ is achieved. The PAIAA element is compact ($0.6\,\lambda \times 0.5\,\lambda$) and can be used in an integrated active array antenna design.

In Chapter 3, it shows that the mutual coupling effects of a multiport integrated active array are more complicated than a passive single-port array antenna. An S-matrix re-normalization procedure is presented consequently to take into accounts both the

mutual coupling effects between the ports within the same element (*intra-element MC*) and the mutual coupling effects between the ports of different elements (*inter-element MC*). The re-normalization procedure is a practical technique to characterize a large-scale PA-integrated active array.

5.2 Future work

It has been demonstrated that the proposed interdisciplinary methodology is an essential asset of PAIAA element design. In the future, the PAIAA element design can be made even more compact by integrating with an MMIC PA developed in-house. The realization of the in-house MMIC PA design also provides an additional degree of freedom by being able to manipulate the PA optimal load impedance by altering the size of the transistor and the bias point. The next step is to scale the integrated active single-element design up to an integrated active array design.

References

[1] *M.2083 : IMT Vision - "Framework and overall objectives of the future development of IMT for 2020 and beyond"*. [Online]. Available: https://www.itu.int/rec/R-REC-M.2083 (visited on 02/25/2020).

[2] Martel Innovate, *5G AND THE FABLE OF THE ELEPHANT*. [Online]. Available: https://www.martel-innovate.com/news/2019/08/26/5g-and-the-fable-of-the-elephant/.

[3] S. Cherry, "Edholm's law of bandwidth", *IEEE Spectr.*, vol. 41, no. 7, pp. 58–60, 2004.

[4] *SILIKA|Silicon-based Ka-band massive MIMO antenna systems for new telecommunication services*. [Online]. Available: http://silika-project.eu/ (visited on 01/29/2020).

[5] C. A. Balanis, *Antenna Theory: Analysis and Design*. John Wiley & Sons, 1997.

[6] Ericsson, "On mm-wave technologies for NR (New Radio)", Tech. Rep. R4-164226, 2016. [Online]. Available: http://www.3gpp.org/ftp/TSG%7B%5C_%7DRAN/WG4%7B%5C_%7DRadio/TSGR4%7B%5C_%7D79/Docs/R4-164226.zip.

[7] M. V. Ivashina, "Joint Design and Co-integration of Antenna-IC Systems", in *2019 13th Eur. Conf. Antennas Propag.*, Krakow, Poland, 2019.

[8] O. A. Iupikov, W. Hallberg, R. Maaskant, C. Fager, R. Rehammar, K. Buisman, and M. V. Ivashina, "A Dual-Fed PIFA Antenna Element with Non-Symmetric Impedance Matrix for High-Efficiency Doherty Transmitters: Integrated Design and OTA-characterization", *IEEE Trans. Antennas Propag.*, vol. 68, no. 1, pp. 21–32, Jan. 2020.

[9] D. Liu, B. Gaucher, U. Pfeiffer, and J. Grzyb, Eds., *Advanced Millimeter-wave Technologies*. Wiley, 2009.

[10] *Integrated Array Antennas (iAA) | Chalmers*. [Online]. Available: `https://www.chalmers.se/en/centres/chaseon/research/Pages/Integrated-Array-Antennas-(iAA).aspx` (visited on 02/13/2020).

[11] *ESA - Spacebus Neo*. [Online]. Available: `https://www.esa.int/Applications/Telecommunications%7B%5C_%7DIntegrated%7B%5C_%7DApplications/Spacebus%7B%5C_%7DNeo` (visited on 02/05/2020).

[12] P. UAV, *Unmanned Aerial Vehicle and Systems*. [Online]. Available: `https://uav-stol.com/`.

[13] P. Khanal, J. Yang, M. Ivashina, A. Hook, and R. Luo, "A wide coverage s-band array with dual polarized connected bowtie antenna elements", in *2019 IEEE Int. Symp. Antennas Propag. Usn. Radio Sci. Meet. APSURSI 2019 - Proc.*, Institute of Electrical and Electronics Engineers Inc., Jul. 2019, pp. 2001–2002.

[14] M. Hashemi, M. Coldrey, M. Johansson, and S. Petersson, "Integrated access and backhaul in fixed wireless access systems", in *IEEE Veh. Technol. Conf.*, vol. 2017-Septe, Institute of Electrical and Electronics Engineers Inc., Feb. 2018.

[15] H. M. Cheema and A. Shamim, "The last barrier: On-chip antennas", *IEEE Microw. Mag.*, vol. 14, no. 1, pp. 79–91, 2013.

[16] N. G. Alexopoulos, P. B. Katehi, and D. B. Rutledge, "Substrate Optimization for Integrated Circuit Antennas", *IEEE Trans. Microw. Theory Tech.*, vol. 31, no. 7, pp. 550–557, 1983.

[17] B. B. Adela, P. T. M. Van Zeijl, U. Johannsen, and A. B. Smolders, "On-Chip Antenna Integration for Millimeter-Wave Single-Chip FMCW Radar, Providing High Efficiency and Isolation", *IEEE Trans. Antennas Propag.*, vol. 64, no. 8, pp. 3281–3291, 2016.

[18] J. J. Lin, H. T. Wu, Y. Su, L. Gao, A. Sugavanam, J. E. Brewer, and K. O. Kenneth, "Communication using antennas fabricated in silicon integrated circuits", in *IEEE J. Solid-State Circuits*, vol. 42, Aug. 2007, pp. 1678–1686.

[19] K. T. Chan, A. Chin, Y. B. Chen, Y. D. Lin, T. S. Duh, and W. J. Lin, "Integrated antennas on Si, proton-implanted Si and Si-on-quartz", *Tech. Dig. - Int. Electron Devices Meet.*, pp. 903–906, 2001.

[20] A. Rashid, S. Watanabe, and T. Kikkawa, "High transmission gain integrated antenna on extremely high resistivity Si for ULSI wireless interconnect", *IEEE Electron Device Lett.*, vol. 23, no. 12, pp. 731–733, Dec. 2002.

[21] R. Wu, W. Deng, S. Sato, T. Hirano, N. Li, T. Inoue, H. Sakane, K. Okada, and A. Matsuzawa, "A 60-GHz efficiency-enhanced on-chip dipole antenna using helium-3 ion implantation process", in *Eur. Microw. Week 2014 Connect. Futur. EuMW 2014 - Conf. Proceedings; EuMC 2014 44th Eur. Microw. Conf.*, IEEE, Oct. 2014, pp. 108–111.

[22] R. Wang, Y. Sun, M. Kaynak, S. Beer, J. Borngraber, and J. C. Scheytt, "A micromachined double-dipole antenna for 122-140 GHz applications based on a SiGe BiCMOS technology", in *IEEE MTT-S Int. Microw. Symp. Dig.*, IEEE, Jun. 2012, pp. 1–3.

[23] A. Babakhani, S. Member, X. Guan, and A. Komijani, "A 77-GHz Phased-Array Transceiver With On-Chip Antennas in Silicon: Receiver and Antennas", *IEEE J. Solid-State Circuits*, vol. 41, no. 12, pp. 2795–2806, 2006.

[24] Y. P. Zhang, Y. Hwang, and G. X. Zheng, "A gain-enhanced probe-fed microstrip patch antenna of very high permittivity", *Microw. Opt. Technol. Lett.*, vol. 15, no. 2, pp. 89–91, Jun. 1997.

[25] A. Barakat, A. Allam, R. K. Pokharel, H. Elsadek, M. El-Sayed, and K. Yoshida, "Compact size high gain AoC using rectangular AMC in CMOS for 60 GHz millimeter wave applications", in *IEEE MTT-S Int. Microw. Symp. Dig.*, 2013.

[26] X.-Y. Bao, Y.-X. Guo, and Y.-Z. Xiong, "60-GHz AMC-Based Circularly Polarized On-Chip Antenna Using Standard 0.18 μm CMOS Technology", *IEEE Trans. Antennas Propag.*, vol. 60, no. 5, pp. 2234–2241, 2012.

[27] M. E. De Cos, Y. Álvarez, and F. Las-Heras, "Planar Artificial Magnetic Conductor: Design and Characterization Setup in the RFID SHF Band", *J. Electromagn. Waves Appl.*, vol. 23, no. 11-12, pp. 1467–1478, 2009.

[28] M. K. Hedayati, A. Abdipour, R. S. Shirazi, M. John, M. J. Ammann, and R. B. Staszewski, "A 38 GHz on-chip antenna in 28-nm CMOS using artificial magnetic conductor for 5G wireless systems", in *Conf. Millimeter-Wave Terahertz Technol. MMWaTT*, 2017, pp. 29–32.

[29] A. Barakat, A. Allam, R. K. Pokharel, H. Elsadek, M. El-Sayed, and K. Yoshida, "Performance optimization of a 60 GHz Antenna-on-Chip over an Artificial Magnetic Conductor", in *2012 Japan-Egypt Conf. Electron. Commun. Comput.*, IEEE, Mar. 2012, pp. 118–121.

[30] A. J. Van Den Biggelaar, U. Johannsen, and A. B. Smolders, "Assessment on the bandwidth of artificial magnetic conductors for antenna-on-chip applications", in *IET Conf. Publ.*, vol. 2018, Institution of Engineering and Technology, 2018.

[31] Dino Flore, *5G-NR workplan for eMBB*. [Online]. Available: `https://www.3gpp.org/news-events/3gpp-news/1836-5g%7B%5C_%7Dnr%7B%5C_%7Dworkplan` (visited on 03/09/2017).

[32] Y. Zhang and J. Mao, "An Overview of the Development of Antenna-in-Package Technology for Highly Integrated Wireless Devices", *Proc. IEEE*, vol. 107, no. 11, pp. 2265–2280, Nov. 2019.

[33] U. Johannsen, "Technologies for integrated millimeter-wave antennas", PhD thesis, 2013.

[34] A. J. Simmons and D. G. Bodnar, "Gain of Active Antenna Systems: Antenna Standards Committee Requests Input", *IEEE Antennas Propag. Soc. Newsl.*, vol. 31, no. 5, p. 62, 1989.

[35] D. M. Pozar, "Microwave Engineering", in *Microw. Eng.* 2005, p. 542.

[36] R. Maaskant, "Deep integration: A paradigm shift in the synthesis of active antenna systems", in *2017 IEEE Int. Symp. Antennas Propag. Usn. Natl. Radio Sci. Meet.*, IEEE, Jul. 2017, pp. 1033–1034.

[37] R. Maaskant, O. A. Iupikov, C. A. H. M. van Puijenbroek, W.-C. Liao, M. Matters-Kammerer, M. V. Ivashina, "Deep Integration Antenna Array: Design Philosophy and Principles", in *2019 13th Eur. Conf. Antennas Propag.*, 2019.

[38] K. C. Gupta and P. S. Hall, Eds., *Analysis and Design of Integrated Circuit – Antenna Modules*. John Wiley & Sons, Inc., 2000.

[39] A. Emadeddin and B. L. Jonsson, "On direct matching and efficiency improvements for integrated array antennas", in *Proc. 2019 21st Int. Conf. Electromagn. Adv. Appl. ICEAA 2019*, Institute of Electrical and Electronics Engineers Inc., Sep. 2019, pp. 408–411.

[40] Y. Qin, S. Gao, and A. Sambell, "Broadband High-Efficiency Circularly Polarized Active Antenna and Array for RF Front-End Application", *IEEE Trans. Microw. Theory Tech.*, vol. 54, no. 7, pp. 2910–2916, 2006.

[41] Y. Chung, C. Y. Hang, S. Cai, Y. Qian, C. P. Wen, K. L. Wang, and T. Itoh, "AlGaN/GaN HFET Power Amplifier Integrated With Microstrip Antenna for RF Front-End Applications", *IEEE Trans. Microw. Theory Tech.*, vol. 51, no. 2 II, pp. 653–659, 2003.

[42] C. Y. Hang, W. R. Deal, Y. Qian, and T. Itoh, "High-Efficiency Push-Pull Power Amplifier Integrated with Quasi-Yagi Antenna", *IEEE Trans. Microw. Theory Tech.*, vol. 49, no. 6, pp. 1155–1161, 2001.

[43] N. Hasegawa and N. Shinohara, "C-Band Active-Antenna Design for Effective Integration With a GaN Amplifier", *IEEE Trans. Microw. Theory Tech.*, pp. 1–8, 2017.

[44] N. Demirel, Y. Pinto, C. Calvez, D. Titz, C. Luxey, C. Person, D. Gloria, D. Belot, D. Pache, and E. Kerherve, "Codesign of a PA-Antenna Block in Silicon Technology for 80-GHz Radar Application", *IEEE Trans. Circuits Syst. II Express Briefs*, vol. 60, no. 4, pp. 177–181, 2013.

[45] E. Öjefors, E. Sönmez, S. Chartier, P. Lindberg, C. Schick, A. Rydberg, and H. Schumacher, "Monolithic Integration of a Folded Dipole Antenna With a 24-GHz Receiver in SiGe HBT Technology", *IEEE Trans. Microw. Theory Tech.*, vol. 55, no. 7, pp. 1467–1474, 2007.

[46] Y. Song, Y. Wu, J. Yang, Y. Tian, W. Tong, Y. Chen, C. Wang, X. Tang, J. Benedikt, and K. Kang, "A Compact Ka-band Active Integrated Antenna with a GaAs Amplifier in a Ceramic Package", *IEEE Antennas Wirel. Propag. Lett.*, 2017.

[47] Y. C. Chen, H. H. Chen, T.-G. Ma, and K.-Y. Lin, "K-band Active Antenna Integrated With CMOS Adaptive-bias Power Amplifier", *Proc. 2015 IEEE 4th Asia-Pacific Conf. Antennas Propagation, APCAP 2015*, pp. 427–428, 2016.

[48] C.-H. Wang, Y.-H. Cho, C.-S. Lin, H. Wang, C.-H. Chen, D.-C. Niu, J. Yeh, C.-Y. Lee, and J. Chern, "A 60GHz Transmitter with Integrated Antenna in 0.18μm SiGe BiCMOS technology", *ISSCC*, vol. 52, no. 2, pp. 305–312, 2006.

[49] Ericsson, "Ericsson Technology Review: Microwave Backhaul Beyond 100 GHz", Tech. Rep., 2017. [Online]. Available: `https://www.ericsson.com/en/reports-and-papers/ericsson-technology-review/articles/microwave-backhaul-evolution-reaching-beyond-100ghz`.

[50] *Qorvo TGF2942 DC - 25 GHz, 2 Watt, 28 V GaN RF Transistor*, `https://www.qorvo.com/products/d/da005920`, Accessed: 2016-08-09.

[51] *Modelithics Qorvo MVP Model Listing - Modelithics, Inc.* [Online]. Available: `https://www.modelithics.com/mvp/qorvo` (visited on 02/05/2020).

[52] *PathWave Advanced Design System (ADS) | Keysight*. [Online]. Available: `https://www.keysight.com/se/en/products/software/pathwave-design-software/pathwave-advanced-design-system.html` (visited on 02/05/2020).

[53] M. Roberg and Z. Popović, "Analysis of High-Efficiency Power Amplifiers With Arbitrary Output Harmonic Terminations", *IEEE Trans. Microw. Theory Tech.*, vol. 59, no. 8, pp. 2037–2048, 2011.

[54] F. H. Raab, "Based Upon a Finite Number of Harmonics", *IEEE Trans. Microw. Theory Tech*, vol. 49, no. 8, pp. 1462–1468, 2001.

[55] W. C. Liao, R. Maaskant, T. Emanuelsson, V. Vassilev, O. Iupikov, and M. Ivashina, "A Directly Matched PA-Integrated K-Band Antenna for Efficient mm-Wave High-Power Generation", *IEEE Antennas Wirel. Propag. Lett.*, vol. 18, no. 11, pp. 2389–2393, 2019. [Online]. Available: `https://ieeexplore.ieee.org/document/8811583/`.

[56] B. L. G. Jonsson, C. I. Kolitsidas, and N. Hussain, "Array Antenna Limitations", *IEEE Antennas Wirel. Propag. Lett.*, vol. 12, pp. 1539–1542, 2013.

[57] C. Craeye and D. González-Ovejero, "A review on array mutual coupling analysis", *Radio Sci.*, vol. 46, no. 2, pp. 1–25, 2011.

[58] R. Maaskant and E. E. M. Woestenburg, "Applying the active antenna impedance to achieve noise match in receiving array antennas", *IEEE Antennas Propag. Soc. AP-S Int. Symp.*, pp. 5889–5892, 2007.

[59] M. Ivashina, R. Maaskant, and B. Woestenburg, "Equivalent System Representation to Model the Beam Sensitivity of Receiving Antenna Arrays", *IEEE Antennas Wirel. Propag. Lett.*, vol. 7, pp. 733–737, 2008.

[60] K. F. Warnick, M. V. Ivashina, R. Maaskant, and B. Woestenburg, "Unified Definitions of Efficiencies and System Noise Temperature for Receiving Antenna Arrays", *IEEE Trans. Antennas Propag.*, vol. 58, no. 6, pp. 2121–2125, Jun. 2010.

[61] E. E. M. Woestenburg, L. Bakker, and M. V. Ivashina, "Experimental Results for the Sensitivity of a Low Noise Aperture Array Tile for the SKA", *IEEE Trans. Antennas Propag.*, vol. 60, no. 2, pp. 915–921, Feb. 2012.

[62] K. F. Warnick, R. Maaskant, M. V. Ivashina, D. B. Davidson, and B. D. Jeffs, *Phased Arrays for Radio Astronomy, Remote Sensing, and Satellite Communications*. Cambridge University Press, Jul. 2018, pp. 155–178. [Online]. Available: `https://www.cambridge.org/core/product/identifier/9781108539258/type/book`.

[63] D. S. Prinsloo, R. Maaskant, M. V. Ivashina, and P. Meyer, "Mixed-mode sensitivity analysis of a combined differential and common mode active receiving antenna providing near-hemispherical field-of-view coverage", *IEEE Trans. Antennas Propag.*, vol. 62, no. 8, pp. 3951–3961, 2014.

[64] K. Kurokawa, "Power Waves and the Scattering Matrix", *IEEE Trans. Microw. Theory Tech.*, vol. 13, no. 2, pp. 194–202, Mar. 1965.

Part II

Included Papers